Submission to the Astrophysical Journal on October 1, 2008
Preprint typeset using LaTeX style emulateapj v. 25/04/01

INTERACTING GALAXIES IN THE A901/902 SUPERCLUSTER WITH STAGES

Amanda Heiderman[1], Shardha Jogee[1], Irina Marinova[1], Eelco van Kampen[9], Marco Barden[9], Chien Y. Peng[5,6], Catherine Heymans[12], Meghan E. Gray[2], Eric F. Bell[4], David Bacon[7], Michael Balogh[8], Fabio D. Barazza[3], Asmus Böhm[10], John A.R. Caldwell[16], Boris Häussler[2], Knud Jahnke[4], Kyle Lane[2], Daniel H. McIntosh[13], Klaus Meisenheimer[4], Sebastian F. Sánchez[11], Rachel Somerville[4], Andy Taylor[12], Lutz Wisotzki[10], Christian Wolf[14], & Xianzhong Zheng[15]
Submission to the Astrophysical Journal on October 1, 2008

ABSTRACT

We present a study of interacting galaxies and the influence of environment in the Abell 901/902 supercluster at $z \sim 0.165$, based on 762 bright, intermediate mass ($M_V \leq -18; M > 1 \times 10^9\ M_\odot$) galaxies. We use *HST* ACS F606W data from the STAGES survey, COMBO-17, *Spitzer* 24μm and XMM-Newton X-ray data. We use visual classification, as well as quantitative CAS parameters to estimate the fraction ($f_{\rm int}$) of interacting galaxies, which are likely candidates for interactions of stellar mass ratio $M_1/M_2 > 1/10$. Our results are: (1) We find, based on visual classification, that $f_{\rm int}$ is $5.0 \pm 1.3\%$, with at least 1.6±0.6% being major interactions ($1/4 < M_1/M_2 \leq 1$), at least $1.0 \pm 0.4\%$ being minor interactions ($1/10 < M_1/M_2 \leq 1/4$), and 2.4±0.7% being ambiguous cases of major or minor interactions. (2) The interacting galaxies are found to lie outside the cluster core: this is likely due to the large galaxy velocity dispersion in that region. Instead, they lie at 0.25 Mpc $< R \leq 1.2$ Mpc, between the core and viral radius. In this region, the estimated frequency and number density of mergers are similar to those seen at typical group overdensities in N-body simulations of accreting groups in the A901/902 clusters. (3) For interacting galaxies, the fraction of galaxies on the blue cloud is 61±14% (23/38) versus 35±7% (251/720) for non-interacting galaxies, implying that interacting galaxies are preferentially blue in A901/902. (4) The average SFR, based on UV or/and IR data, is enhanced by a factor of ~ 1.2 to 3 in interacting galaxies compared to non-interacting galaxies. However, interacting galaxies only contributes $\sim 20\%$ of the total SFR density in the A901/902 clusters, while the rest of the SFR density comes from non-interacting galaxies.

Subject headings: Galaxies: Interactions, Galaxies: Evolution, Galaxies: Formation, Galaxies: Structure, Galaxies: Clusters: General, Galaxies: Clusters: Individual (A901, A902), Galaxies: Clusters: Individual: Alphanumeric: A901, Galaxies: Clusters: Individual: Alphanumeric: A902

1. INTRODUCTION

Understanding how galaxies evolve in various environments (field, groups, and clusters), and as a function of redshift is a key step toward developing a coherent picture of galaxy evolution. Present-day cluster and field galaxies differ due to several factors, which are often grouped under the umbrella of 'nature' versus 'nurture'. Firstly, in cold dark matter (CDM) cosmogonies, the first galaxies formed and evolved early in cluster cores, as the higher initial overdensities led to faster gravitational collapse and more rapid mergers of proto-galaxies (e.g., Cole et al. 2000; Steinmetz & Navarro 2002). Secondly, in the context of the bottom-up CDM assembly paradigm, the outer parts of clusters and superclusters, grow at late times via mergers, smooth accretion, and discrete accretion of groups and field galaxies. This idea is supported by observa-

[1] Department of Astronomy, University of Texas at Austin, 1 University Station C1400, Austin, TX 78712-0259
[2] School of Physics and Astronomy, The University of Nottingham, University Park, Nottingham NG7 2RD, UK
[3] Laboratoire d'Astrophysique, École Polytechnique Fédéralede Lausanne (EPFL), Observatoire, CH-1290 Sauverny, Switzerland
[4] Max-Planck-Institut für Astronomie, Königstuhl 17, D-69117, Heidelberg, Germany
[5] NRC Herzberg Institute of Astrophysics, 5071 West Saanich Road, Victoria, V9E 2E7, Canada
[6] Space Telescope Science Institute, 3700 San Martin Drive, Baltimore, MD 21218, USA
[7] Institute of Cosmology and Gravitation, University of Portsmouth, Hampshire Terrace, Portsmouth, PO1 2EG, UK
[8] Department of Physics and Astronomy, University Of Waterloo, Waterloo, Ontario, N2L 3G1, Canada
[9] Institute for Astro- and Particle Physics, University of Innsbruck, Technikerstr. 25/8, A-6020 Innsbruck, Austria
[10] Astrophysikalisches Insitut Potsdam, An der Sternwarte 16, D-14482 Potsdam, Germany
[11] Centro Hispano Aleman de Calar Alto, C/Jesus Durban Remon 2-2, E-04004 Almeria, Spain
[12] The Scottish Universities Physics Alliance (SUPA), Institute for Astronomy, University of Edinburgh, Blackford Hill, Edinburgh, EH9 3HJ, UK
[13] Department of Astronomy, University of Massachusetts, 710 North Pleasant Street, Amherst, MA 01003, USA
[14] Department of Astrophysics, Denys Wilkinson Building, University of Oxford, Keble Road, Oxford, OX1 3RH, UK
[15] Purple Mountain Observatory, National Astronomical Observatories, Chinese Academy of Sciences, Nanjing 210008, PR China
[16] University of Texas, McDonald Observatory, Fort Davis, TX 79734, USA

tional studies (e.g., Zabludoff & Franx 1993; Abraham et al. 1996a; Balogh, Navarro & Morris 2000), which suggest clusters continuously grew by the accretion of groups. Thirdly, the dominant physical processes affecting galaxies differ in cluster and field environments due to the different galaxy number density, galaxy velocity dispersion, and intracluster medium (ICM) density. Among these processes are close galaxy-galaxy interactions, such as strong tidal interactions and mergers (e.g., Barnes 1992; Moore et al. 1998) and galaxy harassment (e.g., Moore et al. 1996), which stems from the cumulative effect of weak interactions. Furthermore, in clusters where the hot ICM makes up as much as 15% of the total mass, galaxy-ICM interactions, such as ram pressure stripping (Gunn & Gott 1972; Larson et al. 1980; Quilis et al. 2000; Balogh, Navarro & Morris 2000), can play an important role in removing the diffuse gas from galaxies. The tidal field of the cluster potential may also play a relevant role in the dynamical evolution of cluster galaxies (Gnedin 2003).

Systematic studies of the differences between cluster, group, and field galaxies at different redshifts are needed to shed light on the relative importance of these different processes in different environments. Several differences have been observed between galaxies in the field and those in the rich cluster environment, but the physical drivers behind these variations are still under investigation. At $z \sim 0$, the relative percent of massive early type (E+S0) galaxies to spirals rises from (10%+10%:80%) in the field to (40%+50%:10%) in the cores of very rich clusters, leading to the so-called morphology density relation (Dressler 1980; Dressler et al. 1997). However, recent Sloan Digital Sky Survey (SDSS) studies suggest that masses and star formation (SF) histories of galaxies are more closely related to galaxy environment than are their structural properties (Blanton et al. 2005). The SF histories of galaxies depend on both luminosity (Cole et al. 2001) and environment (Diaferio et al. 2001; Koopmann & Kenney 2004). The fraction of blue galaxies in clusters appears to rise with redshift, also know as the Butcher Oemler effect (Butcher & Oemler 1978; Margoniner et al. 2001; de Propis et al. 2003). There is also evidence that SF in bright (M_v < -18) cluster galaxies is suppressed compared to field galaxies (e.g., Balogh et al. 1998, 1999), for reasons that are not well understood.

Merging of cluster galaxies has been proposed as a mechanism for the change in galaxy populations in clusters from that of the field (e.g., Toomre & Toomre 1972; Lavery & Henry 1988; Lavery Pierce, & McClure 1993). Understanding the influence of the cluster environment on the rate of galaxy interactions will allow us to set constraints on the importance of interactions. There have been various studies on the properties of galaxies (e.g., Dressler 1980, Postman & Geller 1984, Giovanelli, Haynes, & Chincarini, 1986, Kennicutt 1983; Gavazzi & Jaffe 1985, Whitmore et al. 1993) and also on galaxy interactions (e.g., Lavery & Henry 1988; Lavery, Pierce, & Mclure 1992; Zepf 1993; Dressler et al. 1994; Couch et al. 1998; van Dokkum et al. 1998a, 1999; Tran et al. 2005b, 2008) in different environments. The former studies suggest that galaxy interactions may play a role in morphological transformations of galaxies in clusters, but there have been few systematic studies of interactions in clusters that utilized high resolution *HST* images as well as *Spitzer* 24μm, and X-ray images. With a resolution of 0.1$''$ or 300 pc at $z = 0.17$, the *HST* images (Gray et al. 2008) allow for the identification of interaction signatures such as double nuclei, arcs, and shells. *Spitzer* 24μm imaging (Bell et al. 2005, 2007) enables for the study of the obscured star formation and X-ray maps (Gilmour et al. 2007; Grey et al. 2008, in prep) provide information of how the ICM densities change throughout the cluster.

In this paper we present a study of the frequency, distribution, color, and SF properties of strong galaxy interactions and the influence of environment in the A901/902 supercluster at $z \sim 0.165$. We use *HST* ACS F606W data taken as part of the Space Telescope A901/902 Galaxy Evolution Survey (STAGES; Gray et al. 2008), *Spitzer* 24μm data (Bell et al. 2005, 2007), XMM-Newton X-ray data (Gilmour et al. 2007), dark matter (DM) mass measurements from weak lensing (Heymans et al. 2008), and ground based COMBO-17 imaging data (Wolf et al. 2004). The dataset provides high resolution ACS-based morphologies, stellar masses, accurate spectrophotometric redshifts, gravitational lensing maps, and SF rates.

We present the data and sample selection in § 2. An outline of the two different methods that we used to identify interacting galaxies: a physically motivated visual classification system (Jogee et al. 2008a,b) complemented with spectrophotometric redshifts, and the CAS criterion ($A > 0.35$ and $A > S$) based on CAS asymmetry A and clumpiness S parameters (Conselice et al. 2000) , are in § 3.2 and § 3.3. In § 4.1 and 4.2, we explore the frequency of interacting galaxies in A901/902 based on these two methods and present one of the first systematic comparisons to date between CAS-based and visual classification results in clusters. We set a lower limit on the fraction of major (those with mass ratio $M1/M2 \geq 1/4$) mergers/interactions. In § 4.3, we examine the distribution of interacting galaxies in the A901/902 supercluster as a function of clustocentric radius, galaxy number density, local galaxy surface density (Σ_{10}), relative ICM density, and local DM mass surface density. In § 4.4, we compare our results to expectations based on analytical estimates and simulations. In § 4.5, we compare our results on the A901/902 supercluster to groups and clusters at different redshifts out to $z \sim 0.8$. We investigate the fraction of interacting and non-interacting galaxies on the blue cloud and red sequence as a function of clustocentric radius in § 4.6. Finally in § 4.7, we compare the star formation rate (SFR) of interacting and non-interacting cluster galaxies. The results of this work are summarized in § 5.

We assume a flat cosmology with $\Omega_m = 1 - \Omega_\lambda = 0.3$ and $H_0 = 70$ km s^{-1} Mpc^{-1} throughout this paper.

2. THE A901/902 SUPERCLUSTER: DATASET AND SAMPLE SELECTION

The A901/902 supercluster is composed of three clusters: A901a, A901b, and A902, and related groups (Gray et al. 2002; Heymans et al. 2008). This study utilizes data from the STAGES survey (Gray et al. 2008), which provides high resolution F606W *Hubble Space Telescope* (*HST*) Advanced Camera for Surveys (ACS) images over a $0.5^\circ \times 0.5^\circ$ field. Additional multi-wavelength data include XMM-Newton (Gilmour et al. 2007, Gray et al. 2008b),

Spitzer 24μm data (Bell et al. 2005, 2007), and ground based COMBO-17 imaging data (Wolf et al. 2004).

Accurate spectrophotometric redshifts and spectral energy distributions, based on 5 broad bands ($UBVRI$) and 12 medium band filters, are available from the COMBO-17 project (Wolf et al. 2004). Stellar masses are taken from Borch et al. (2006). They were derived by fitting the 17-band COMBO spectral energy distributions (SEDs) with a library of template SEDs, which were constructed using the PEGASE stellar population synthesis model, assuming different SF histories and a Kroupa (Kroupa, Tout, & Gilmore 1993) initial mass function (IMF) in the mass regime 0.1–120 $M_{\odot}$. Such stellar masses are consistent within 10% with masses estimated using a Kroupa (2001) or Chabrier (2003) IMF[17].

The ACS F606W images have an effective point spread function (PSF) of $\sim$0.1″, which corresponds to $\sim$280 pc at $z \sim 0.165$ for our assumed cosmology. Thus, they provide high resolution deep images enabling us to resolve structural components such as disks, bars, bulges, spiral arms, and interaction features such as double nuclei, arcs, shells, tails, tidal debris, and accreting satellites.

Using the spectrophotometric redshifts ($\delta_z/(1+z) \sim 0.02$ down to $R_{\rm Vega}$ of 23), we have a sample of 786 bright ($M_{\rm V} \leq$ -18) galaxies. The estimated field contamination for this sample is $\leq$ 15%. We chose the cut of $M_{\rm V} \leq$ -18 because E to Sd galaxies tend to dominate the cluster luminosity function in this luminosity range (Binggeli, Sandage, & Tammann 1988), while dwarf galaxies dominate at lower luminosities. We emphasize that these luminosity cuts are only meant to provide a separation between regimes dominated by dwarf and non-dwarf galaxies, rather than a case-by-case identification of the two galaxy types. We have also analyzed faint (-18 $< {\rm M_V} \leq -15.5$) galaxies, but we only present the robust results for the bright sample for the following reasons. Many morphological properties (§ 3) can be more accurately characterized in E to Sd galaxies than in smaller lower luminosity dwarf galaxies, given the ACS PSF of $\sim$280 pc at the cluster redshift. Furthermore, a larger degree of contamination from field galaxies arises at lower luminosities. We further restrict our bright galaxy sample to include galaxies above the stellar mass completeness limit ($M \gtrsim 1 \times 10^9 M_{\odot}$; 762 galaxies) at the supercluster redshift. The magnitude distribution of the final sample is shown in Fig. 1.

3. METHODOLOGY AND ANALYSIS

3.1. *Interacting galaxies in this study*

Before outlining the methods (§ 3.2 and § 3.3) that we use to identify interacting galaxies, we briefly discuss the different types of interactions that are of interest to our study.

According to simulations, galaxy interactions of mass ratio $M_1/M_2 > 1/10$ tend to have a significant impact on galaxy evolution. They include major interactions, which are defined to be those with a mass ratio of $1/4 < M_1/M_2 \leq 1/1$, as well as minor interactions with $1/10 < M_1/M_2 \leq 1/4$. Simulations show that major mergers of stellar systems typically destroy the outer disks, transforming them via violent relaxation, into systems with an $r^{1/4}$ de Vaucouleurs-type stellar profile, such as ellipticals (e.g., Negroponte & White 1983; Barnes & Hernquist 1991; Mihos & Hernquist 96; Struck 1997; Naab & Burkert 2001). However, it is to be noted that in some gas-rich major mergers, a disky component can form or survive inside the resulting spheroidal component (Hopkins et al. 2008), producing a remnant whose overall profile is less steep than de Vaucouleurs. Irrespective of the details, the different simulations suggest that ongoing/recent major mergers are associated with arcs, shells, ripples, tidal tails, large tidal debris, extremely asymmetric light distributions, double nuclei inside a common body, galaxies linked via tidal bridges of light, and galaxies enclosed within the same distorted envelope of light.

Conversely, minor interactions involving a spiral and a smaller satellite will not destroy the outer disk of the spiral (e.g., Hernquist & Mihos 1995; Smith et al. 1997; Jogee et al. 1999). Typically, the smaller companion sinks via dynamical friction, may excite warps, bars, spirals, and other non-axisymmetric perturbations, and leads to vertical heating, arcs, shells, ripples, tidal tails, tidal debris, warps, offset rings, and highly asymmetric light distributions (e.g., Quinn et al. 1993; Hernquist & Mihos 1995; Mihos et al. 1995; Quinn, Hernquist, & Fullagar 1993; Smith et al. 1997; Jogee et al. 1999; Jogee 2006 and references therein).

In this paper, we identify interacting systems using the aforementioned morphological signatures seen in simulations. We consider such interacting systems to be likely candidates for an ongoing or recent interaction of mass ratio $M_1/M_2 > 1/10$. We utilize two independent methods to identify interacting galaxies. The first is a physically motivated visual classification system (§ 3.2) similar to that developed in Jogee et al. (2008a,b). The second method uses the CAS criterion ($A > 0.35$ and $A > S$), which is based on quantitative asymmetry (A), and clumpiness (S) parameters (§ 4.2) derived using the CAS code (Conselice et al. 2000).

3.2. *Visual classification of interacting and non-interacting galaxies*

We visually classify F606W images of the sample of 762 bright ($M_{\rm V} \leq$ -18), intermediate mass ($M \geq 1 \times 10^9 M_{\odot}$) galaxies in the A901/902 supercluster. A small fraction (below 1%) could not be classified due to image defects, low signal to noise, and a highly compact appearance.

Our visual classification scheme is illustrated in Fig. 2. We identify interacting galaxies using the morphological signatures suggested by the simulations of mass ratio $M_1/M_2 > 1/10$ outlined in § 3.1. The interacting galaxies (Fig. 2) are assigned the visual class 'Int', and fall in two groups:

- 'Int Type 1': This first group is composed of 47% (18/38) of interacting systems that host *externally-triggered* distortions, similar to those identified in the aforementioned simulations. These post-merger signatures include tidal tails, shells, ripples, warps, strongly asymmetric tidal debris and distortions in the disk, and double nuclei inside a common envelope. 'Int Type 1' galaxies are unambiguous cases of

[17] We adopt a Chabrier (2003) IMF when exploring the contribution of mergers to the SFR (§ 4.7)

interacting galaxies, since they exhibit the morphological distortions induced by a strong gravitational disturbance. In particular, note that a strongly distorted galaxy is counted as 'Int Type 1', irrespective of whether it has a readily visible companion. Furthermore, most 'Int Type 1' systems have morphology consistent with post-mergers such that these systems are counted as one galaxy merger (§ 4.4).

- 'Int Type 2': This class includes the rest of strongly interacting galaxies. A galaxy is assigned an 'Int Type 2' class if it shows no strong morphological distortions, but is indicative of late merger phase due to having a companion which satisfies three criteria: the companion is overlapping or in contact with the galaxy of interest, such that the two galaxies share a common envelope of light; it has the same COMBO-17 spectrophotometric redshift within the accuracy $\delta_z/(1+z) \sim 0.02$ (§ 2); and its stellar mass ratio satisfies $M_1/M_2 > 1/10$. While the classification of a galaxy as 'Int Type 2' depends on spectrophotometric redshift, it is to be noted that 'Int Type 2' systems are very unlikely to be be line-of-sight chance projection as the projected separation d of the two galaxies is typically < 10 kpc. This is a smaller separation than that used in the identification of close pairs, where d is $\lesssim$20-30 kpc. Most 'Int Type 2' systems are in the late phases of an ongoing merger and both galaxies are counted as a single merger system when counting the number of mergers (§ 4.4).

The remaining galaxies show no indication of a recent strong interaction and are classified as non-interacting (Fig. 4). They are subdivided into two classes: Irr-1 and Symmetric:

- 'Non-interacting Irr-1' galaxies refer to galaxies that exhibit *internally-triggered* asymmetries, typically on scales of a few hundred parsecs. These asymmetries are generally due to stochastic SF and/or low ratios of rotational to random velocities (Fig. 4). They can impart a clumpy morphology to a galaxy and are different from externally-driven distortions, such as tails and ripples, which are often correlated on scales of several kpc.

- 'Non-interacting symmetric' galaxies are relatively undistorted and are not associated with any overlapping companion.

Several tests were performed on the visual classes. The visual classifications (VC) were calibrated by having three classifiers (AH, IM, SJ) train on a set of a few hundred nearby field and A901/902 cluster galaxies. The full supercluster sample was then classified by AH and IM, with all ambiguous cases and interacting galaxies discussed by all three classifiers for final determination. Random checks on sub-samples of galaxies were performed by SJ. The dispersion (D) between classifiers is taken to be the fractional difference between classifiers ($\delta f_{\rm VC}/f_{\rm VC}$), resulting in 4%, 19%, 16% for Non-interacting Symmetric, Non-interacting Irr-1, and Interacting classes. We adopt a dispersion of 20% on the mean $f_{\rm VC}$, as a measure of the inherent subjectivity in the visual classification. All errors in $f_{\rm VC}$ for our analysis are taken to be the addition of the dispersion between classifiers ($f_{\rm VC}\times$D) and the binomial error in the fraction ($\sqrt{f_{\rm VC}(1-f_{\rm VC})/N_{\rm VC}}$).

3.3. *CAS: Quantitative method for capturing interacting galaxies*

Using the CAS code (Conselice et al. 2000, Conselice 2003a), quantitative structural parameters measuring the concentration (C), asymmetry (A), and clumpiness (S) were derived for the supercluster galaxies. CAS was run on the F606W images and the segmentation maps produced during the original source extraction (Caldwell et al. 2008) were used to mask neighboring galaxies.

The concentration index (Bershady et al. 2000) corresponds to a measure of the ratio of 80 to 20 percent of the curve of growth radii contained in 1.5 times the Petrosian inverted radius at r($\eta = 0.2$) on five times the logarithmic scale:

$$\mathrm{C} = 5 \times \log(\mathrm{r}_{80\%}/\mathrm{r}_{20\%}). \quad (1)$$

The other two CAS parameters, asymmetry A and clumpiness S, are also measured within $1.5 \times$ r($\eta = 0.2$) radius. The asymmetry parameter is measured by subtracting a galaxy's image from that image rotated 180 degrees from the galaxy's center and normalizing by the summation of the absolute value of the residual intensity. The clumpiness parameter is a quantitative measure of the high spatial frequency patchiness of a galaxy. It is defined as the summation of the difference of the galaxy's original flux and the flux of an image with the high frequency structures muted by smoothing over a filter on order of the clumpiness, taking into account the background flux over that same area. This measurement is then divided by the summation of the original flux of the galaxy to obtain the clumpiness parameter (S).

Conselice et al. (2000) argue that the CAS merger criterion ($A > S$ and $A > 0.35$) at $\lambda_{\rm rest} > 4500$ Å , can be used to capture galaxies which have have strong asymmetries indicative of major mergers. However, calibrations of the asymmetry value with N-body simulations (Conselice 2006) have shown that for galaxies involved in major mergers of mass ratios 1:1 to 1:3, the asymmetries vary as a function of time during the interaction. The A value reaches a peak near the midpoint of the interaction and falls off both before and after this time to less than 0.35. The criterion A>0.35 is fulfilled only $\sim$1/3 of the time for major mergers in these simulations while minor mergers of mass ratios below 1:5 have A values significantly lower than this criterion. In effect, in intermediate mass field galaxies at $z \sim 0.24$ to 0.80, recent work (Jogee et al. 2008a,b; Miller et al. 2008) shows that the CAS criterion typically only picks up 50% to 70% of galaxies visually typed as being disturbed or interacting. Furthermore, at rest-frame wavelengths bluer than the B-band, A has a significant contamination from non-interacting dusty star-forming galaxies. These results caution against using CAS blindly without complementary visual classifications.

The effectiveness of the CAS criterion has not been explored in cluster environments where the dominant galaxy population is gas-poor. In § 4.1, we present the interaction fraction ($f_{\rm CAS}$) from CAS and perform one of the first

systematic comparisons to date between CAS-based and visual classification results in clusters. When citing $f_{\rm CAS}$, we adopt error bars computed by taking the systematic errors in CAS A and S to obtain the high and low error bars on the number of galaxies the CAS criterion picks up.

4. RESULTS AND DISCUSSION

4.1. *Frequency of interacting galaxies in A901/902 from visual classification*

The results of the visual classifications are shown in Table 1, Fig. 3, and Fig. 4. The fraction in terms of percent of interacting galaxies is 38/762 or 5.0±1.3% among bright, intermediate mass ($M_{\rm V} \leq -18$, $M > 1\times 10^9\ M_\odot$) galaxies in A901/902.

The systems visually classified as interacting galaxies are likely candidates for interactions of mass ratio $M_1/M_2 > 1/10$ (§ 3.2). When comparing observational results to theoretical predictions or simulations, it is often desirable to separate interacting galaxies into major ($1/4 < M_1/M_2 \leq 1/1$) versus minor ($1/10 < M_1/M_2 \leq 1/4$) interactions. But in practice, for many interacting galaxies, it is not possible to unambiguously make this distinction. since the exact level of morphological disturbances induced depends not only on the mass ratio of the progenitors, but also on the orbital geometry (prograde or retrograde), the gas mass fraction, and structural parameters (e.g., Mihos & Hernquist 1996; Struck 1997; Naab & Burkert 2001; Mihos et al. 1995, di Matteo et al. 2007).

In effect, many signatures could be caused by both major and minor interactions. Thus, we divide the interacting systems into three categories: major, minor, and major/minor interactions. The last category includes ambiguous cases that could be either major or minor, while the first two categories are clear cases of major and minor interactions, respectively. They allow us to set lower limits to the major and minor merger fraction.

We consider major interactions as those galaxies that show unique tell-tale morphological signatures or indicators. These include close pairs of galaxies, whose members have a mass ratio $1/4 < {\rm M_1/M_2} \leq 1$, spectrophotometric redshifts match within the accuracy $\delta_{\rm z}/(1+z) \sim 0.02$, and are connected by a bridge or common envelope (Fig. 2, cases 9-11 & 13-16), and/or have a 'train-wreck' type morphology (Fig. 2, case 12).

For galaxies of class 'Int Type 2', we identify minor interactions using the same redshift criterion as above, but restrict the mass ratios of the companion to $1/10 < {\rm M_1/M_2} \leq 1/4$. We also include galaxies of class 'Int Type 1', which host an extended surviving disk with signs of a strong recent interaction, but do not have an overlapping companion of mass ratio $> 1/4$ with similar photometric redshift. The latter condition ensures that we do not capture the early phases of a major merger when the disks of the merging galaxies are starting to get distorted before they merge. The signs of strong interactions in the outer disk include a warp, prominent tidal debris and tails, and strong large-scale asymmetries.

The results are shown in Table 2 and Fig. 3. We estimate that at least 1.6±0.6% of the galaxies in our sample are undergoing a major interaction, at least 1.0±0.4% are undergoing minor interactions, and 2.4±0.7% are undergoing major or minor interactions.

4.2. *Frequency of interacting galaxies in A901/902 from CAS*

CAS results for the A901/902 supercluster sample are shown in Table 3 and Figures 5 and 6. If CAS, is used instead of visual classification, the fraction $f_{\rm CAS}$ of strongly distorted galaxies is 19/762 or $2.5^{+1.7\%}_{-0.1\%}$. This is a factor of two lower than the visually-based interaction fraction $f_{\rm VC}$.

However, the comparisons of $f_{\rm CAS}$ and $f_{\rm VC}$ do not tell the whole story, as the nature of the systems picked by the two methods can be quite different. The visual types of the 19 systems captured by the CAS criterion is shown in Table 3. About 6/19 ($33^{+24\%}_{-4\%}$) of the CAS mergers turn out to be non-interacting systems, as shown by Fig. 5 and Table 3. Fig. 6 shows examples of these contaminants: they tend to be dusty highly inclined galaxies and systems with low level asymmetries that seem to be caused by SF. The remaining 13 CAS mergers are visually classified as interacting.

It is also useful to ask what fraction of the visually-identified interacting galaxies meet the CAS criterion. In effect, the CAS criterion only captures 13 of the 38 ($34^{+5\%}_{-0\%}$) visually-identified interacting galaxies (Fig. 5). Fig. 6 shows examples of interacting galaxies missed by CAS : the missed systems include galaxies with fainter outer tidal features, double nuclei where CAS puts the center between the nuclei, and pairs of very close connected galaxies.

Since the CAS criterion is widely used to pick major mergers, it is interesting to ask if it has a significantly higher capture fraction for the interacting galaxies that we consider major mergers. This is not found to be the case as the CAS merger criterion recovers 5/12 ($42^{+0\%}_{-0\%}$) of major interactions. It is also interesting to note that the CAS criterion recovers 0/8 (0%) of galaxies classified as minor interactions. The remaining systems that the CAS criterion recovers is 8/18 or $44^{+13\%}_{-0\%}$ of the major/minor interactions, which have no mass dependence.

4.3. *Distribution of interacting galaxies*

In order to define different regions of the A901a, A901b, and A902 clusters, we computed the projected bright galaxy ($M_V < -18$) number density n as a function of clustocentric radius R (Fig. 7) by assuming a spherical distribution. Note here that each galaxy is assigned to the cluster closest to it, and R is measured from the center of that cluster. As shown by Table 6, the A901 clusters have central galaxy number densities n (1100 to 1800 galaxies ${\rm Mpc}^{-3}$), which are intermediate to that of the rich Coma cluster and the more diffuse Virgo cluster.

We consider the cluster core to be at $R \leq 0.25$ Mpc, as this is the region where the projected number density n rises very steeply (Fig. 7). The cluster virial radii are taken to be ~ 1.2 Mpc, based on estimates from the dark matter maps derived from gravitational lensing by Heymans et al. (2008). Throughout this paper, we refer to the region which is located at 0.25 Mpc $< R \leq 1.2$ Mpc between the cluster core and the cluster virial radius as the 'outer region of the cluster'. The region outside the virial radius (1.2 Mpc $< R \leq 2.0$ Mpc) is referred to as

the 'outskirt region of the cluster'. The core, outer region, and outskirt region are labeled on Fig. 7.

Fig. 8 shows the distribution of interacting galaxies in the A901a, A901b, and A902 clusters. These galaxies lie outside the cluster core. Most (34/38 or 89±5%) are located in the outer region of the cluster (0.25 Mpc $< R \leq$ 1.2 Mpc), and 11±5% in the outskirt region (1.2 Mpc $< R \leq$ 2.0 Mpc). Using the volume of the core region, and a spherical shell of the outer region and outskirt of the cluster, the number density of interacting galaxies ($n_{\rm merg}$) varies from 0 to 1.2 to 0.025 galaxies Mpc^{-3} (Table 7).

Fig. 9 show the values of various environmental parameters for interacting and non-interacting galaxies at different clustocentric radii. Following Wolf et al. (2005) and Gilmour et al. (2007), we define and compute the local galaxy surface density (Σ_{10}) as the number of galaxies per (Mpc/h)$^{-2}$ that are in an area defined by a circle of radius containing the average distance to the 9th and 10th nearest neighbor. The DM mass surface density κ is computed locally using the coordinates of each galaxy on the weak lensing map provided by Heymans et al. (2008). The relative local ICM counts are measured at each galaxy position using the X-ray map from Grey et al. (2008b) and Gilmour et al. (2007). Since the interacting galaxies lie preferentially in the outer region of the cluster (0.25 Mpc $< R \leq$ 1.2 Mpc), they are associated with low values of κ and intermediate values of Σ_{10}, and ICM density (Fig. 9).

4.4. *What accounts for the distribution of interacting galaxies?*

The timescale for collisions and close encounters is given by:

$$t_{coll} = \frac{1}{n\sigma_{gal}A}, \tag{2}$$

where n is the galaxy number density, $\sigma_{\rm gal}$ is the galaxy velocity dispersion, A is the collisional cross section, $\pi f(2r_{gal})^2$, r_{gal} is a typical galaxy radius, and f is the gravitational focusing factor (Binney & Tremaine, 1987). Since the average velocity dispersion in clusters is high, the value for f will be low and we will assume it to be on order of unity. Thus,

$$t_{coll} \sim 800 \times \left(\frac{n}{1000 \quad \rm Mpc^{-3}}\right)^{-1} \times \left(\frac{\sigma}{1000 \quad \rm km \quad s^{-1}}\right)^{-1} \times \left(\frac{\rm r_{gal}}{10 \quad \rm kpc}\right)^{-2} \rm Myr. \tag{3}$$

We compute n using the same method as in § 4.3 for the core, and use spherical shells to compute the n in the outer region, and cluster outskirt. The local galaxy velocity dispersion profiles for A901a/b, A902, and SWG from kinematic modeling using ∼ 300 2dF redshifts (Gray et al. in prep.) are shown in Fig. 10, and average velocity dispersions, $\sigma_{\rm gal}$ are shown in Table 6.

The central galaxy velocity dispersion within the cores ($R <$ 0.25 Mpc) of A901a,b and A902 typically range from 700 to 1000 km s^{-1}. Outside the cluster core, in the outer region (0.25 Mpc $< R \leq$ 1.2 Mpc), the small number statistics leads to large error bars on the galaxy velocity dispersion, making it un-viable to determine whether it remains high, drops, or rises. For the sake of estimating timescales, we take the average $\sigma_{\rm gal}$ for A901/902 to be ∼ 800 km s^{-1} in three regions of the cluster. The timescales (t_{coll}) for close encounters are shown in Table 7 and range from 0.844 to 12.6 to 244 Gyrs from the core ($R \leq$ 0.25 Mpc), to the outer region (0.25 Mpc $< R \leq$ 1.2 Mpc), and outskirt region (1.2 Mpc $< R \leq$ 2.0 Mpc) of the cluster.

It may at first seem surprising that interacting galaxies do not preferentially lie in the cluster core, where the probability for close encounters is high due to the associated short value of the timescale t_{coll} for collisions and close encounters. However, if the galaxy velocity dispersion (σ_{gal}) is large, a close encounter is unlikely to lead to a merger or a large amount of tidal damage (i.e. to strong morphological and kinematical distortions). This is because a large galaxy velocity dispersion will likely cause the energy E of the reduced particle in a binary encounter to be positive, causing the orbit to become unbound (Binney & Tremaine, 1987).

Most of the interacting galaxies lie at a projected clustocentric radius of 0.25 Mpc $< R \leq$ 1.2 Mpc, between the core and viral radius although in this region the timescale for collisions and close encounters is quite large. We suggest two possible reasons why strong interactions and mergers might populate this outer region. The first possibility is that the velocity dispersion of galaxies falls between the core and outer region, due to the *intrinsic* velocity dispersion profile of the clusters. Many clusters show a flat velocity dispersion profile from 1 Mpc outward, but several also show a declining profile (den Hartog & Katgert 1996, Carlberg 1997). In the latter cases, the velocity dispersions can fall from 1500 to 100 km s^{-1} from the cluster core to outer region of the cluster. Since the velocity local dispersion profiles in the regions of interest in the A901/902 (Fig. 10) are based on a small number of galaxies and therefore large errors in σ_{gal}, we cannot determine if the velocity dispersion profile falls or remains flat. An additional difficulty is that the member galaxies of the neighboring clusters influence σ_{gal} at ∼ 0.5 Mpc for A901a/b and ∼ 1 Mpc for A902.

The second possibility is that the interacting galaxies are part of groups or field galaxies that are being accreted along filaments by the A901/902 clusters. This would be in line with the idea that clusters continuously grow by mergers and accretion of groups (e.g., Zabludoff & Franx 1993; Abraham et al. 1996a; Balogh, Navarro & Morris 2000). Groups have lower galaxy velocity dispersion (typically below 300 km s^{-1}) than clusters, as shown in Table 7. Furthermore simulations show that merger rates are highest as field galaxies and galaxies in groups accrete into cluster along cosmological filaments (see below; van Kampen & Katgert 1997; Fig. 11).

To further quantify the possibility of groups accreting into the A901/A902 clusters, we compare the data to model predictions from simulations of the STAGES A901/A902 supercluster (van Kampen et al. 2008, in prep). The simulation aims to reproduce the environment as observed for A901/A902 by using constrained initial conditions that produce clusters with similar *overall* properties like A901, A902, and the neighboring A907 and A868. The simulation box is large enough to contain all

these, and hence reproduce the overall large-scale density and velocity fields similar to what is observed. A phenomenological galaxy formation model is then used to simulate the galaxy population in the same box, allowing us to select mock galaxies on luminosity and stellar mass as done in the observed dataset. A stellar mass cut of ($M > 1\times 10^9\ M_\odot$) is applied in the simulations, corresponding to the observational sample mass cut. The solid lines in Fig. 11 shows the predicted number density (n) and fraction (f) of galaxy mergers with mass ratio $M_1/M_2 > 1/10$, as a function of environment, as characterized by the local overdensity ($\delta^{\rm G}$). The latter is is calculated by smoothing the density of dark matter halos with a Gaussian of width 0.4 Mpc to take out the effect of individual galaxies. Typical values of $\delta^{\rm G}$ are $\sim$ 10-100 for group overdensities, ~ 200 at the cluster virial radius, and $\gtrsim 1000$ in the core of rich clusters.

Typically, in the simulations, as field and group galaxies fall into a cluster along filaments, the coherent bulk flow enhances the galaxy density and causes galaxies to have small relative velocities, thus leading to a high probability for mergers at typical group overdensities. Closer to the cluster core, galaxies show large random motions rather than bulk flow motion, leading to a large galaxy velocity dispersion, and a sharp drop in the probability of mergers. Hence, as shown in Fig. 11, the highest number density of mergers is found at group overdensities, while at overdensities typical of the cluster core, the number density and fraction of mergers drop sharply.

In order to compare the data to simulation results, we first compute the number of mergers ($N_{\rm merg}$) using the formula:

$$N_{\rm merg} = N_{\rm Int\ Type\ 1} + \frac{N_{\rm Int\ Type\ 2}}{2}, \qquad (4)$$

where we adapt the division by two in the class 'Int Type 2' in order to be consistent with the simulations and count the two galaxies involved in the interaction as a single merger system. Unlike 'Int Type 1' systems, where the interaction involves galaxies whose individual mass is at least $1\times 10^9\ M_\odot$, 'Int Type 2' systems have $M_1 + M_2 > 2\times 10^9\ M_\odot$.

The solid curve in Fig. 11 shows the merger fraction and number density predicted by the simulations as a function of overdensity. The dashed lines in Fig. 11 show the estimated range in the observational number density ($n_{\rm merg}$) and fraction ($f_{\rm merg}$) of mergers, for the 3 different regions of the A901/902 clusters. The points at which the dashed lines cross the solid curve tell us the typical overdensities at which we expect to find such merger fraction or densities in the simulations. It can be seen that the low merger density seen in the core region of the cluster correspond to those expected at typical cluster core overdensities. On the other hand, the larger merger density we observe between the cluster core and the virial radius (0.25 Mpc $< R \leq 1.2$ Mpc) is close to those seen in typical *group overdensities*. This is in agreement with the above scenario, whereby the accretion of field and/or group galaxies along filaments, where they have low relative velocities and enhanced overdensities, leads to enhanced merger rates.

We note, however, several caveats in the comparison. In comparing our data to simulations, we directly compare projected values of number density or fraction of mergers from two dimensional observations, to the predicted number density of mergers from three dimensional simulations. The projection effect can introduce uncertainties in our observational estimate. Another caveat is that we do not have a more complete suite of simulations.

A further indirect evidence for group accretion stems from comparing semi-analytic galaxy catalogs to STAGES observations. Rhodes et al. (in prep.) finds an overabundance in galaxies in A902 compared to its mass. This could be explained by two or more galaxy groups in projection, providing further evidence for group accretion.

4.5. *Comparison with groups and clusters at different epochs*

We first recapitulate the results of this study (§ 4.1). In the A901/902 clusters, we find the fraction of interacting galaxies is 38/762 or 5.0±1.3% and most of these systems have $M_{\rm V} \sim$ -19 to -22 and $L \leq L^*$. We estimate that at least 1.6±0.6% being major interactions ($1/4 < M_1/M_2 \leq 1$), at least 1.0±0.4% being minor interactions ($1/10 < M_1/M_2 \leq 1/4$), and 2.4±0.7% being ambiguous cases of major or minor interactions.

Next, we compare our observed fraction of interacting galaxies with studies of other clusters and group galaxies out to $z \sim 0.8$, over the last 7 Gyr (Fig. 12). These comparisons are difficult to make as different studies employ different luminosity or mass cutoffs. Furthermore, some studies consider only major mergers, while others consider all interacting galaxies, which are likely candidate for both major and minor interactions.

The variation in galaxy populations sampled at different epochs must also be kept in mind when comparing results at lower redshift with those at out to $z \sim 0.8$. Samples of galaxies at low redshift will contain a representative amounts of both faint ($L \leq L^*$) and luminous ($L > L^*$) galaxies. Higher redshift samples, on the other hand, will contain an over-representative number of $L > L^*$ galaxies due to sampling a larger volume and detection limits undersampling the fainter galaxy population.

There have been several studies of galaxy interactions at intermediate redshift clusters (Lavery & Henry 1988; Lavery, Pierce, & Mclure 1992; Dressler et al. 1994; Oemler, Dressler, & Butcher 1997; Couch et al. 1998), but only few to date with high resolution *HST* imaging. Couch et al. (1998) used WFPC/WFPC2 observations and spectroscopy of two clusters at $z \sim$0.3 and $\sim$ 0.4 (R$\sim$22.5; $L < L^*$ galaxies). In this study they classified $\sim$7/200 or $\sim$ 3.5% galaxies to be merging based on separations and visible distortions. The interacting systems in these two intermediate redshift clusters are found to be typically blue. These points are shown on Fig. 12. We note that the interacting galaxies in these two clusters are quite similar to those in A901/902. In both cases, they tend to be blue and preferentially in the outskirts. Furthermore, for the absolute magnitude range ($M_{\rm V} \sim$-19 to -22) of the A901/902 sample, the fraction of blue interacting galaxies is $\sim$ 60% (§ 4.6). This is comparable to the fraction ($\sim$ 60%) of blue interacting galaxies in the $L < L^*$ sample of these the A901/902 clusters.

A study by Dressler et al. (1994) of a $z \sim 0.4$ cluster and was observed using the WFPC camera and the frac-

tion of bright ($M_V < -18.5$) galaxies identified as merger products or possible tidal interactions, respectively, was 10/135 and 14/135. Another study of four clusters at $z = 0.37 - 0.41$ by Oemler, Dressler, & Butcher (1997) placed a lower limit of 5% on the fraction of interacting or merging galaxies with $M_V < -19$ or $L \leq L^*$ also using WFPC.

A high redshift ($z = 0.83$) cluster was studied by van Dokkum et al. (1999) *HST* WFPC2 images and spectroscopic redshifts with 80 confirmed members. They found a high number (17%) of luminous ($M_B \sim -22$; $L \sim 2L^*$) systems that exhibit signatures of merging systems. These mergers were found to be red, bulge dominated, and are located in the outskirts of the cluster. A later study by Tran et al. (2005b) used spectroscopic followup to confirm that 15.7±3.6% of these mergers were bound pairs with separations $\lesssim$30h^{-1} kpc and relative velocities $\lesssim$300 km s^{-1}. While these systems are located outside the cluster centers similar to that of interacting systems in A901/902, the galaxy sample at high redshift are dominated by more luminous galaxies ($M_B \sim$ -22; $L \sim 2L^*$) than galaxies in the A901/902 sample where most galaxies have $M_V \sim$ -19.5 to -22 (Fig. 1). The number statistics for bright ($\sim 2L^*$) interacting galaxies in A901/902 are not robust enough to allow for comparison with the van Dokkum et al. (1999) fraction of interacting galaxies.

Finally, we look at the fraction of interacting galaxies in *groups*. A study by McIntosh et al. (2007) finds that ∼1.5% of massive ($M \geq 5 \times 10^{10} M_\odot$) galaxies in SDSS groups (with $M_{\rm halo} > 2.5 \times 10^{13}\ M_\odot$) are major mergers at z of 0.01 to 0.12. Most of the systems are mergers between two red sequence galaxies and are found to lie between 0.2-0.5 Mpc from the group center. A study by McGee et al. (2008) also find an enhancement in asymmetric bulge-dominated group galaxies, consistent with a higher probability for merging in the group environment. Additional evidence for mergers in groups is shown in a study of a supergroup at $z \sim 0.37$ by Tran et al. (2008), which they finds dry dissipationless mergers and signatures thereof in 3 of 4 brightest group galaxies.

A merger fraction of of 6% was found by Zepf (1993) in Hickson compact groups at $z < 0.05$, which have a luminosities that are $L \leq L^*$. The merger fraction is significantly higher than that in SDSS groups. The increased merger fraction is expected as Hickson compact groups are different from loose groups because compact groups have high number densities comparable to those in cluster cores, but low galaxy velocity dispersions. These two conditions provide an environment most favorable to strong tidal interactions and mergers, as argued in § 4.4.

More systematic, high resolution, studies of galaxy interactions in both high and low redshift clusters with spectroscopically confirmed members are needed to better understand differences in the fraction of interacting galaxies throughout time. Increased merger rate at higher redshifts ($z \sim$1) may be due to clusters being in the process of formation. Also, mergers may have been more important in the evolution of cluster galaxies at earlier times. The low fraction of interacting galaxies among the intermediate mass range of ($M = 1 \times 10^9$ to a few $\times 10^{10} M_\odot$) or intermediate luminosities ($L < L^*$) of galaxies seen in the A901/902 supercluster and other intermediate redshift clusters suggests that in the later stages of cluster evolution, interactions may play a less important role in the transformation of cluster galaxies.

4.6. *Galaxies on the blue cloud and red sequence*

Fig. 13 shows the rest-frame $U-V$ color plotted against stellar masses for galaxies of different visual classes: Interacting, Non-interacting Irr-1, and Non-interacting Symmetric. For visually classified galaxies in our sample, we find that 274 lie on the blue cloud. Out of the 38 visually classified interacting systems, 23/38 or 61 ± 14% (23/38) lie on the blue cloud. Conversely, out of 720 visually classified non-interacting galaxies, 251/720 or 35 ± 7% are on the blue cloud. The fraction of interacting galaxies on the blue cloud ($f_{\rm int-BC}$) is about two times larger than the fraction of non-interacting galaxies ($f_{\rm non-int-BC}$) on the blue cloud, implying that interacting galaxies are preferentially blue compared to non-interacting ones. The distribution of non-interacting galaxies on the blue cloud increases from 9±4% to 37±7% to 40±9% (Table 7; Fig. 13) from the cluster core ($R \leq 0.25$ Mpc), to the outer region (0.25 Mpc $< R \leq$ 1.2 Mpc), and to the outskirt region (1.2 Mpc $< R \leq$ 2.0 Mpc). Correspondingly, the fraction of interacting galaxies on the blue cloud from core to outer region to the cluster outskirt is 0% to 62±15% to 50±25% (Table 7). This large fraction of blue interacting galaxies in these regions may be due to the enhanced SFR in interacting galaxies (see § 4.7). It may also be the result of the interacting galaxies being part of accreted groups (§ 4.4) that are bluer than the average cluster galaxy.

Out of the 38 interacting galaxies, 23 lie on the blue cloud and 15 are on the red sequence. What is the nature of the interacting galaxies on the red sequence? We find that 4/15 interacting galaxies on the red sequence are candidates for 'dry' tidal interactions and mergers, with a smooth appearance, suggestive of gas-poor systems (e.g., case 16 in Figure 3). The remainder of interacting systems on the red sequence are dusty red galaxies (e.g., cases 6 and 14 Figure 3). We note that Wolf et al. (2008) reports a significant population ∼ 180 red dusty galaxies in A901/902 and the dusty red interacting galaxies here only account for only ∼ 3% (6/180) of this population.

4.7. *SF properties of interacting galaxies*

This work uses SFRs based on UV from COMBO-17 (Wolf et al. 2004) and *Spitzer* 24μm derived by Bell et al. (2005, 2007). The unobscured SFR$_{\rm UV}$ is derived using the 2800 Å rest frame luminosity ($L_{\rm UV} = 1.5 \nu l_{\nu,2800}$) as described in Bell et al. (2005, 2007). The UV spectrum is dominated by continuum emission from massive stars and provides a good estimate of the integrated SFR from the younger stellar population in the wavelength range of 1216-3000 Å. The SFR$_{\rm IR}$ is derived using the 24μm flux to construct the integrated IR luminosity ($L_{\rm IR}$) over 8-1000μm following the methods of Papovich & Bell (2002). The total SFR is derived using identical assumptions of Kennicutt (1998) from PEGASE assuming a 100 Myr old stellar population with constant SFR and a Chabrier (2003) IMF:

$$\rm SFR_{UV+IR} = 9.8 \times 10^{-11} (L_{IR} + 2.2 L_{UV}). \quad (5)$$

The factor of 2.2 on the UV luminosity accounts for light being emitted longward of 3000 Å and shortward of 1216 Å

by young stars. The total SFR accounts for both the dust-reprocessed (IR) and unobscured (UV) star formation. All of our 762 sample galaxies with $M \geq 1 \times 10^9 M_\odot$ have UV-based SFR from COMBO-17 observations. Of this sample, $\sim$ 10% (78/762) were not observed with *Spitzer*, $\sim$ 27% (204/762) were observed and detected at 24μm, while the rest had no detection at the $\sim 4\sigma$ depth of 83 μJy.

The UV-based SFR (SFR_{UV}) is plotted versus stellar mass in Fig. 14 for all 762 galaxies in our sample. The SFR_{UV} ranges from $\sim$ 0.01 to to 4 $M_\odot$ yr^{-1}. The UV-based SFR represents a lower limit to the total SFR for galaxies on the blue cloud and most star-forming galaxies on the red sequence. However, for some old red galaxies, the SFR_{UV} may overestimate the true SFR as the UV light from such systems may not trace massive OB stars, but rather low to intermediate mass stars.

Fig. 15 shows the UV+IR-based SFR (SFR_{UV+IR}). For galaxies with a 24μm detection, we plot SFR_{UV+IR}. The UV+IR-based SFR (Fig. 15) ranges from $\sim$ 0.1 to to 10 $M_\odot$ yr^{-1}. For the 480 galaxies that are observed but undetected, with *Spitzer*, we use the 24μm detection limit as an upper limit on the 24μm flux. These points are shown as inverted triangles. Galaxies without any *Spitzer* coverage are not included in this figure.

In a cluster environment, the competition between processes that enhance the SFR and those that depress the SFR, ultimately determine the average SFR of cluster galaxies. The first class of processes are strong close interactions: tidal and mergers (e.g., Toomre & Toomre 1972), and harassment (e.g., Moore et al. 1996), which refers to the cumulative effect of weak interactions. The second class of processes include ram pressure stripping of cold gas out of the galaxy by the hot ICM (e.g., Gunn & Gott 1972), and strangulation (e.g., Larson et al. 1980; Balogh et al. 2000).

For the few interacting galaxies (orange line) present, the average SFR_{UV} is typically enhanced by a modest factor of only 1.2–2.2 compared to the Non-interacting Symmetric galaxies (purple line) and to all Non-interacting galaxies (i.e Symmetric + Irr-1; black line). Similarly, the UV+IR-based SFR (SFR_{UV+IR}; and Fig. 15) of interacting galaxies is typically enhanced by only a factor of $\sim$ 2 to 3 compared to the Non-interacting Symmetric galaxies (purple line) and to all Non-interacting galaxies (i.e Symmetric + Irr-1; black line). We note that a similar enhancement in the average SFR, by a factor of 1.5 to 2 from visual classification, and 1.4 to 2.1 with CAS is also found in interacting field galaxies over $z \sim$ 0.24–0.80 by Jogee et al. (2008a,b).

SFR enhancements are also seen in galaxy pair studies in the field (Robaina et al. in prep; Ellison et al. 2008) and in different environments (Alonso 2004). An enhanced SFR in strong galaxy interactions is expected, since interactions lead to large supercritical gas surface densities via shocks and via gravitational torques, which drive and pile gas into the central regions. This modest enhancement is consistent with that found by di Matteo et al. (2007; see their Fig. 10), based on a recent statistical study of several hundred galaxy collisions.

While galaxy interactions in the A901/902 clusters enhance the SFR of individual galaxies, it is clear that they do not contribute much to the total SFR of the cluster. This minimal contribution to the total cluster SFR is due to the low number of interacting galaxies in A901/902, and the fact that these interactions only cause a modest SFR enhancement. In effect, only 20% of the total UV and UV+IR SFR density of the A901/902 clusters comes from interacting galaxies.

5. SUMMARY

We present a study of interacting galaxies and the influence of environment in the A901/902 supercluster at $z \sim 0.165$ based on 762 bright , intermediate mass ($M_V \leq$ -18; $M > 1 \times 10^9$ $M_\odot$) galaxies. We use *HST* ACS F606W data from the STAGES survey, COMBO-17, *Spitzer* 24μm and XMM-Newton X-ray data. We use visual classification, as well as quantitative CAS parameters to estimate the fraction ($f_{\rm int}$) of interacting galaxies, which are likely candidates for interactions of stellar mass ratio $M_1/M_2 > 1/10$. Our findings are:

- The fraction of interacting galaxies (§ 4.1) is 38/762 or 5.0±1.3% among bright, intermediate mass ($M_V \leq$ -18; $M \geq 1\times 10^9$ $M_\odot$) cluster galaxies in A901/902. We estimate that at least 1.6±0.6% are major interactions ($1/4 < M_1/M_2 \leq 1$), at least 1.0±0.4 are minor interactions ($1/10 < M_1/M_2 \leq 1/4$), and 2.4±0.7% are ambiguous cases of major or minor interactions.

- If CAS is used (§ 4.3) instead of visual classification, the fraction of highly distorted galaxies is 19/762 or $2.5^{+1.7\%}_{-0.1\%}$ (Fig. 5). However, the nature of the systems captured by CAS and visual classification can be quite different. CAS only captures 13/38 ($34^{+5\%}_{-0\%}$) of the visually-identified interacting galaxies, and the missed systems include galaxies with double nuclei, or fainter outer tidal features. Furthermore, the remaining 6/19 ($33^{+24\%}_{-4\%}$) of the systems captured by CAS turn out to be non-interacting systems (Table 3). These contaminants tend to be dusty highly inclined galaxies and systems with low level asymmetries that are probably due to star formation.

- Throughout this paper, we consider the core of each cluster to be at a projected clustocentric radius of $R \leq 0.25$ Mpc. We refer to the region between the cluster core and the virial radius as the outer region of the clusters (0.25 Mpc $< R \leq$ 1.2 Mpc). We refer to the region outside the virial radius (1.2 Mpc $< R \leq$ 2.0 Mpc) as the outskirt region of the clusters. The interacting galaxies are found to lie outside the cluster core although the timescale for collisions and close encounters is shortest in the core ($<$ 1 Gyr). We suggest that this is due to the large velocity dispersion (700 to 900 km/s) of galaxies in the core. Such a dispersion makes it less likely that a close encounter between two galaxies culminates into a merger or a disruptive interaction associated with a lot of tidal heating.

  Most of the interacting and mer=ging galaxies lie in the outer region (0.25 Mpc $< R \leq$ 1.2 Mpc), between the core and viral radius, although the timescale for collisions and close encounters is quite

large ($\gg 1$ Gyr) in this region. One possible explanation might be that the galaxy velocity dispersion drops in the outer region, hence favoring mergers. However, limited number statistics of current spectroscopic data do not allow us to assess this possibility. Another possible scenario is that the interacting galaxies in the outer region are part of groups or field galaxies that are being accreted along cosmological filaments by the A901/902 clusters. We find that our estimated frequency and number density of mergers are similar to those seen at typical group overdensities in N-body simulations of groups and field galaxies accreting into A901/902 clusters.

- We compare of our observed fraction of interacting galaxies with studies of other clusters and group galaxies out to $z \sim 0.8$ (§ 4.5). We find no evidence for significant evolution between $z \sim 0.17$ to 0.40 in the fraction of interactions among $L \leq L^*$ cluster galaxies.
- Out of the 38 interacting galaxies, 23 lie on the blue cloud and 15 are on the red sequence (§ 4.6). The fraction of interacting galaxies on the blue cloud is is $61 \pm 14\%$ (23/38), which is about twice as high as the fraction of $35 \pm 7\%$ (251/720) for non-interacting galaxies. This suggests that interacting galaxies are preferentially blue compared to non-interacting ones. This excess of blue galaxies among interacting systems may be due to the enhanced recent SFR in interacting galaxies and/or due to the possibility that the interacting galaxies are part of field or group galaxies, which are accreting into the cluster. Of the remaining 15 interacting galaxies, which lie on the red sequence, we find that 4 are candidates to be 'dry' tidal interactions and mergers, with a smooth appearance, while 6 are dusty red galaxies.
- For the few interacting galaxies present, the average $\mathrm{SFR_{UV}}$ and $\mathrm{SFR_{UV+IR}}$ are typically enhanced by only a modest factor of $\sim$ 1.2-2 and $\sim$ 2 to 3, respectively, compared to the Non-interacting Symmetric galaxies and to all the Non-interacting galaxies (i.e., Symmetric + Irr-1). This modest enhancement is consistent with that found by di Matteo et al. (2007), based on a recent statistical study of several hundred galaxy collisions. However, since only 20% of the total SFR density of the A901/902 clusters comes from interacting galaxies, interactions do not contribute much to the total SFR output of the cluster. A similar SFR enhancement in galaxy interactions is also found in $z \sim 0.24 - 0.8$ field galaxies (Jogee et al. 2008a,b) and in pairs by Robaina et al. (in prep.).

A.H. and S.J. gratefully acknowledge support from NSF grant AST-0607748, LTSA grant NAG5-13063, and HST-GO-10861 and HST-GO-10395 from STScI, which is operated by AURA, Inc., for NASA, under NAS5-26555. We would like to thank Christopher Conselice for his assistance with CAS. E.vK. and M.B. were supported by the Austrian Science Foundation FWF under grant P18416,C.Y.P. by STScI and NRC-HIA Fellowship programmes, C.H. by European Commission Programme Sixth Framework Marie Curie Outgoing International Fellowship under contract MOIF-CT-2006-21891 and a CITA National fellowship, M.E.G by an Anne McLaren Research Fellowship, E.F.B. and K.J. by the DFG's Emmy Noether Programme, A.B. by the DLR (50 OR 0404), S.F.S. by the Spanish MEC grants AYA2005-09413-C02-02 and the PAI of the Junta de Andaluc a as research group FQM322, L.V.W. by NSERC, CIfAR and CFI, C.W. by a PPARC Advanced Fellowship, and D.H.M. by NASA under LTSA Grant NAG5-13102. The STAGES team thanks Hans-Walter Rix for providing essential support contributing to the success of the STAGES project. This research made use of NASA's Astrophysics Data System and NASA/IPAC Extragalactic Database.

REFERENCES

Abraham, R. G., et al. , 1996a, ApJS, 107, 1
Alonso, M. S., et al. , 2004, MNRAS, 352, 1081
Balogh, M. L., et al. , 1998, ApJ, 504, 75
Balogh M. L., et al. , 1999, ApJ, 527, 54
Balogh, M. L., Navarro, J. F., & Morris, S. L. 2000, ApJ, 540, 113
Balogh, M. L., & Morris, S. L., 2000, MNRAS, 318, 703
Barnes, J. E., & Hernquist, L. E., 1991, ApJ, 370, 65
Barnes, J. E., 1992, ApJ, 393, 484
Bell, E., et al. , 2005, ApJ, 625, 23
Bell, E., et al. 2007, ApJ, 663, 834
Bershady, M. A., Jangren, J. A., & Conselice, C. J, 2000, AJ, 119, 2645
Binggeli, B., Tammann, G. A.,& Sandage, A. 1987,AJ, 94, 251
Binggeli, B., Sandage, A., & Tammann, G.A., 1988, ARAA,26, 509
Binney J., Tremaine S., 1987, *Galactic Dynamics*, Princeton Univ. Press, Princeton
Blanton, M. R., et al. 2005, ApJ, 629, 143
Borch, A., et al. 2006, A&A, 453, 869
Butcher, H., & Oemler, A. Jr., 1978,ApJ, 219, 18
Caldwell, J. A. R., et al. , 2008, ApJS, 174, 136
Chabrier, G., 2003, PASP,115, 763
Carlberg, R., G., et al. , 1997, ApJ, 476L, 7C
Cole, S., et al. , 2000, MNRAS, 319, 168
Cole, S., et al. , 2001, MNRAS, 326, 255
Conselice, C. J., Bershady, M. A., & Jangren, A. 2000, 529, 886
Conselice, C. J., 2003, AJ, 126, 1183
Conselice, C. J., 2006, ApJ, 638, 686
Couch, W., et al. 1998, ApJ, 497,188
Diaferio, A., et al. , 2001, MNRAS, 323, 999
Dressler, A., 1980, ApJ, 236, 351
Dressler, A., et al. 1994,, ApJ, 435, 23
Dressler, A., et al. , 1997, ApJ, 490, 577
Ellison, S., L., et al. , 2008, AJ, 135, 1877
Gavazzi, G. & Jaffe, W., 1985, ApJ, 294, 89
Gilmour, R., et al. 2007, MNRAS, 380, 1467
Gilmour et al. 2008, in prep.
Giovanelli, R., Haynes, M. P., & Chincarini, G. L., 1986, ApJ, 300, 77
Gnedin, O. Y. 2003, ApJ, 582, 141
Gray, M. E. , et al. 2002, ApJ, 568, 141
Gray, M. E. , et al. 2008, in preparation.
Gunn, J.E., & Gott, J.R., III, 1972, ApJ, 176, 1
den Hartog, R., & Katgert, P., 1996, MNRAS, 279, 349
Hernquist, L. E.,& Mihos, 1995
Heymans, C. et al. 2008, MNRAS, 385, 1431
Hopkins, P. F., Cox, T. J., Younger, J. D., Hernquist, L., ApJ, submitted (arXiv:0806.1739), 806
Jogee et al. , 1999, ApJ, 526, 665
Jogee, S. 2006, in Physics of Active Galactic Nuclei at all Scales, Lecture Notes in Physics, Vol. 693, Eds. D. Alloin, R. Johnson, and P. Lira (Springer: Berlin Heidelberg), 143 (astro-ph/0408383)
Jogee, S., et al. , 2008a, in Formation and Evolution of Galaxy Disks, ed. J. G. Funes, S. J., & E. M. Corsini (San Francisco: ASP), in press (arXiv:0802.3901)

Jogee, S., Miller, S., Penner, K., Skelton, R. E., Conselice, C. J., Somerville, R. S., and the GEMS collaboration, 2008b, ApJ, submitted
Kennicutt, R. C. Jr., 1983, AJ, 88, 1094
Kennicutt, R. C. Jr., 1998, ARAA, 36, 189
Koopmann, R. A., & Kenney, J. D. P. 2004, ApJ, 613, 866
Kroupa, P. Tout, C. A., & Gilmore, G., 1993, MNRAS, 262, 545
Larson, R. B., Tinsley, B. M., Caldwell, C. N., 1980, ApJ, 237, 692
Lavery, R. J., & Henry, J. P., 1988, ApJ, 330, 596
Lavery, R. J., Pierce, M. J.,& McClure, R. D., ApJ, 1993, 418, 43
McGee, L., M., et al. , 2008, astroph/0804.2693
Naab, T., & Burkert, A., 2001, ApJ, 555, 91
Negroponte, J., & White, S. D. M., 1983, MNRAS, 205, 1009
Margoniner, V. E., et al. , 2001,ApJ, 548, 143
di Matteo, P., et al. , 2007, A&A, 468, 61
McIntosh, D. H., et al. 2008, MNRAS, 388, 1537
Mihos, J. C.,& Hernquist, L., 1996, ApJ, 464, 641
Mihos, J. C., et al. , 1995, ApJ, 438, 75
Miller, S., et al. , 2008, ASP conference proceedings of the "Frank N. Bash Symposium 2007: New Horizons in Astronomy", ed. A., Frebel, J. Maund, J. Shen, M. Siegel, (San Francisco: ASP),393, 235
Moore, B., et al. 1996, Nature, 379, 613
Moore, B., Lake, G., Katz, N., et al. 1998, ApJ, 495, 139
Papovich, C., & Bell, E. F., 2002, ApJ, 579, L1
Postman, M., & Geller, M. J., 1984, ApJ, 281, 95
de Propis, R., et al. , 2003, MNRAS, 345, 725
Quilis, V., Moore, B.,Bower, R., 2000, Science, 288, 1617
Quinn, P. J., Hernquist, L., & Fullagar, D. P., 1993, 403, 74
Rhodes, R., et al. , 2008, in prep.
Robaina, A., et al. , in prep.
Smith, B. J., Curtis, S., Kenney, J. D. P., & Jogee, S. 1999, AJ, 117, 1237
Steinmetz, M., & Navarro, J. F., 2002, New Astronomy, 7, 155
Struck, C., 1997, ApJS, 113, 269
Tago, E. et al. , 2008, A&A, 479,927
The, L., S., & White, S. D. M. , 1986, AJ, 92, 1248
Toomre, A., & Toomre, J., 1972, ApJ, 178, 623
Tran, K.-V., H., et al. , 2005b, ApJL, 627, 25
Tran, K.-V., H., et al. , 2008, astroph/0806.4387
van Dokkum, P. G., et al. 1998a, ApJ, 500, 714
van Dokkum, P. G., et al. 1999, ApJL, 520, 95
van Kampen, E., & Katgert, P., 1997, MNRAS, 289, 327
van Kampen, E., et al. , 2008, in prep.
Whitmore, B., et al. , 1993 ApJ, 407, 489
Wolf, C., et al. 2004, A&A, 421, 913
Wolf, C., Gray, M. E., Meisenheimer, K. 2005, A&A, 443 435
Wolf et al. , 2008, in prep.
Zabludoff , A. I., & Franx, M., 1993, AJ, 106, 1314
Zepf, S. E., et al. 1993, ApJ, 407, 448

TABLE 1
RESULTS BASED ON VISUAL CLASSIFICATIONS

Visual Class (1)	$N_{\rm gal}$ (2)	$f_{\rm gal}$ (3)
Interacting 'Int'	38	0.050±0.01
Non-interacting Irr-1	104	0.14±0.03
Non-interacting Symmetric	616	0.81±0.16
Unclassifiable	4	0.005±0.003

Note. — The results are shown for the sample of 762 bright ($M_{\rm V} \leq$ -18; $M_* \leq 1 \times 10^9 M_\odot$) galaxies. Columns are : (1) Visual class (VC); (2) $N_{\rm gal}$ = Number of galaxies with a given VC.; (3) $f_{\rm gal}$ = Fraction of bright galaxies with a given VC.

TABLE 2
MAJOR AND MINOR INTERACTIONS AMONG INTERACTING GALAXIES

Visual Class (1)	Mass Ratio (2)	$N_{\rm gal}$ (3)	$f_{\rm gal}$ (4)
Major interaction	$1/4 < M1/M2 \leq 1/1$	12	0.016± 0.006
Minor interaction	$1/10 < M1/M2 \leq 1/4$	8	0.01± 0.004
Major or minor interaction	$1/10 < M1/M2 \leq 1/1$	18	0.024±0.007

Note. — This table gives our estimate of the type of interaction, major or minor, which the interacting galaxies in Table 1 are undergoing. Columns are : (1) Visual class; (2) Mass ratio of interaction (3) $N_{\rm gal}$ = Number of galaxies; (4) $f_{\rm gal}$ = Fraction of galaxies.

TABLE 3
VISUAL BREAKDOWN OF GALAXIES SATISFYING CAS CRITERIA: $A > 0.35$ AND $A > S$

Visual Class (1)	$N_{\rm CAS}$ (2)	$f_{\rm CAS}$ (3)
All Visual Types	19	1.00
Interacting 'Int'	13	0.680±0.11
Non-interacting Irr-1	4	0.21±0.09
Non-interacting Symmetric	2	0.11±0.07

Note. — Columns are : (1) Visual Classification (VC); (2) $N_{\rm CAS}$ = = Number of galaxies of a given visual type satisfying the CAS criteria; (3) $f_{\rm CAS}$ = Fraction of galaxies satisfying CAS criteria with a given visual type.

TABLE 4
VISUAL CLASSES OF GALAXIES ON THE BLUE CLOUD AND RED SEQUENCE

Visual Class (1)	$N_{\rm blue}$ (2)	$f_{\rm blue}$ (3)	$N_{\rm red}$ (4)	$f_{\rm red}$ (5)
Interacting 'Int'	23	0.083± 0.02	15	0.031± 0.001
Non-interacting Irr-1	91	0.329± 0.07	13	0.027± 0.009
Non-interacting Symmetric	160	0.578± 0.12	456	0.940± 0.19
Unclassifiable	3	0.01± 0.007	1	0.002± 0.002
All	277	1.0	485	1.0

Note. — The results are shown for the sample of 762 galaxies. Columns are : (1) Visual class; (2) $N_{\rm blue}$ = Number of galaxies on blue cloud; (3) $f_{\rm blue}$ = Fraction of galaxies on blue cloud; (4) $N_{\rm red}$ = Number of galaxies on red sequence; (5) $f_{\rm red}$ = Fraction of galaxies on red sequence

TABLE 5
MAJOR AND MINOR INTERACTIONS ON THE BLUE CLOUD AND RED SEQUENCE

Visual Class (1)	$N_{\rm blue}$ (2)	$f_{\rm blue}$ (3)	$N_{\rm red}$ (4)	$f_{\rm red}$ (5)
Major interaction	6	0.021 ± 0.001	6	0.012± 0.006
Minor interaction	3	0.01 ± 0.007	5	0.01± 0.005
Major or minor interaction	14	0.05 ± 0.02	4	0.008± 0.004
All	277	1.0	485	1.0

Note. — This table gives our estimate of the type of interaction, major or minor, which the interacting galaxies in Table 4 are undergoing. Columns are : (1) Visual Classification; (2) $N_{\rm blue}$ = Number of galaxies on blue cloud; (3) $f_{\rm blue}$ = Fraction of galaxies on blue cloud; (4) $N_{\rm red}$ = Number of galaxies on red sequence; (5) $f_{\rm red}$ = Fraction of galaxies on red sequence;

TABLE 6
COMPARISON OF PROJECTED GALAXY NUMBER DENSITIES n AND σ_{gal}

System	Core $R \leq 0.25$ Mpc (galaxies Mpc^{-3})	Outskirt $R > 1.2$ Mpc (galaxies Mpc^{-3})	$\sigma_{\rm gal}$ (km s^{-1})
Virgo[a]	360	75	400-750
Coma[b]	10000	400	~ 900
A901a[c]	1800	230	890±182
A901b[c]	1100	240	1189±266
A902[c]	1300	170	792±176
Groups[d]	~ 0.01		~ 100

Note. — References for the values cited: a = Binggeli,Tammann, & Sandage (1987); b = The & White (1986); c = number densities from this work, average local velocity dispersions from Gray et al. (2008); d = Tago et al. (2008)

TABLE 7
PROPERTIES IN CORE, OUTER REGION, AND OUTSKIRT OF A901/902 CLUSTERS

	Cluster Core ($R \leq 0.25$ Mpc)	Cluster Outer Region (0.25 Mpc $< R \leq 1.2$ Mpc)	Outskirt (1.2 Mpc $< R \leq 2.0$ Mpc)
(1) N	77	570	107
(2) $N_{\rm non-int}$	77	536	103
(3) $N_{\rm int}$	0	34	4
(4) Volume V (Mpc^3)	0.065	7.17	26.3
(5) n (gal Mpc^{-3})	1185	79.5	4.1
(6) $\langle B-V \rangle$	0.852	0.759	0.756
(7) $\langle U-V \rangle$	1.29	1.08	1.07
(8) t_{coll} (Gyr)	0.844	12.6	244
(9) $N_{\rm merg}$	0	25	2
(10) $n_{\rm merg}$ (gal Mpc^{-3})	0	1.2	0.025
(11) $f_{\rm merg}$	0	0.043	0.018
(12) $N_{\rm major-merg}$	0	6	0
(13) $n_{\rm major-merg}$ (gal Mpc^{-3})	0	0.28	0
(14) $f_{\rm major-merg}$	0	0.01	0
(15) $N_{\rm minor-merg}$	0	3	1
(16) $n_{\rm minor-merg}$ (gal Mpc^{-3})	0	0.14	0.01
(17) $f_{\rm minor-merg}$	0	0.005	0.009
(18) $N_{\rm non-int-BC}$	7	199	41
(19) $f_{\rm non-int-BC}$	0.09	0.37	0.40
(20) $N_{\rm int-BC}$	0	21	2
(21) $f_{\rm int-BC}$	0	0.62	0.5

Note. — This table shows galaxy properties and timescales in three different regions of the cluster: the core ($R \leq 0.25$ Mpc), the outer region (0.25 Mpc $< R \leq 1.2$ Mpc) between the core and the cluster, and the outskirt region (1.2 Mpc $< R \leq 2.0$ Mpc). Only bright ($M_V \leq -18$) intermediate mass ($M > 1\times 10^9\ M_\odot$) galaxies are considered. See § 4.3 for details. The rows are : (1) N: No. of galaxies ; (2) $N_{\rm non-int}$: No. of non-interacting galaxies; (3) $N_{\rm int}$: No. of interacting galaxies; (4) V: Projected Volume; (5) n: Projected number density of galaxies; (6) $B-V$: Mean $B-V$ rest frame color; (7) $U-V$: Mean $U-V$ rest frame color; (8) $t_{\rm coll}$: Timescale for collisions or close encounters; (9) $N_{\rm merg}$: No. of mergers from Equation 4 (10) $n_{\rm merg}$: Projected number density of interacting galaxies (11) $f_{\rm merg}$: Fraction of interacting galaxies. (12)-(14): same as (9)-(11), but for major mergers with a mass ratio ($1/4 < M1/M2 \leq 1/1$); (15)-(17): same as (9)-(11), but for minor mergers with a mass ratio ($1/10 < M1/M2 \leq 1/4$); (18) $N_{\rm non-int-BC}$: No. of non-interacting galaxies on blue cloud; (19) $f_{\rm non-int-BC}$: Fraction of non-interacting galaxies on blue cloud; (20) $N_{\rm int-BC}$: No. of interacting galaxies on blue cloud; (21) $f_{\rm int-BC}$: Fraction of interacting galaxies on blue cloud;

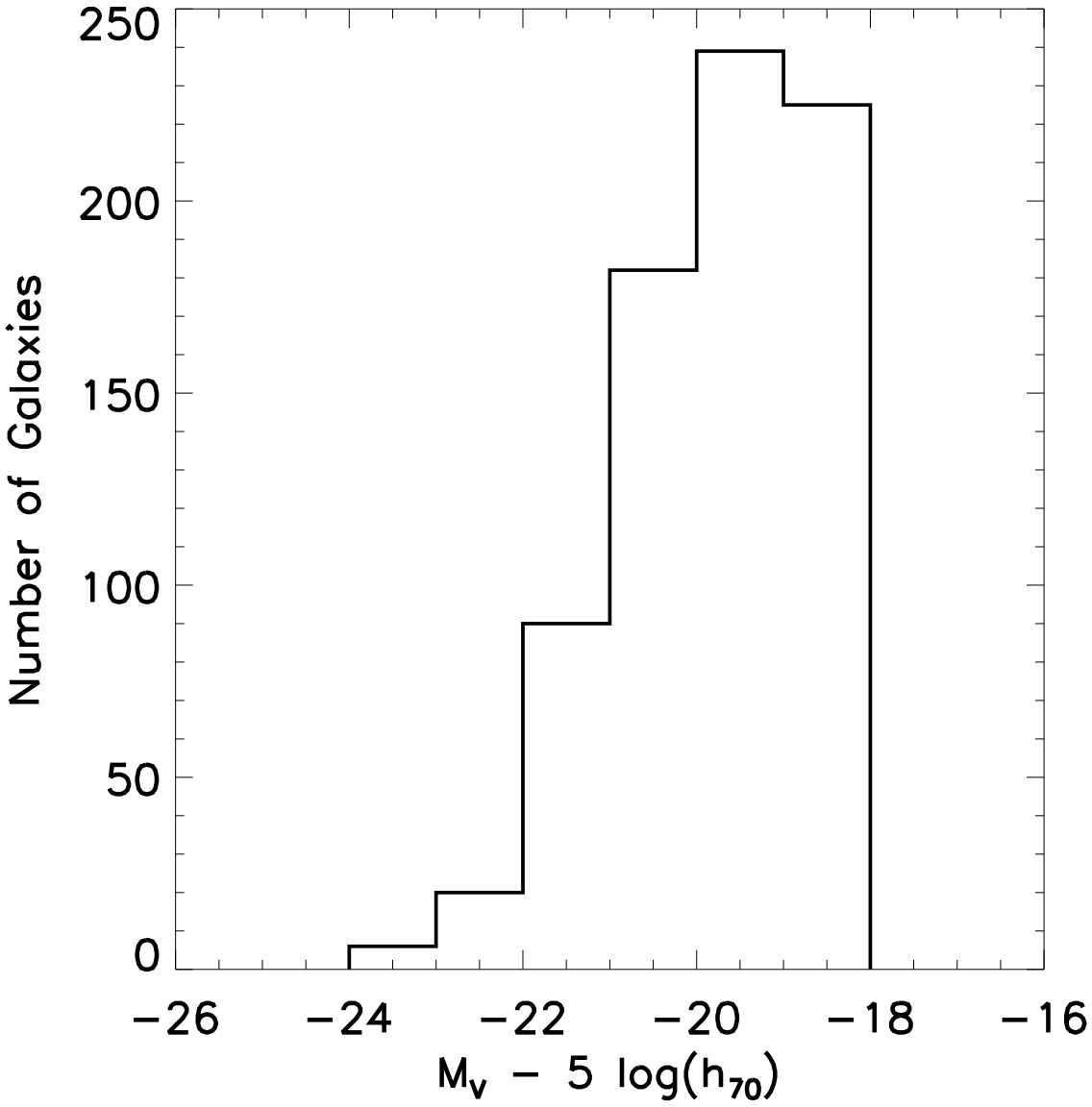

FIG. 1.— Absolute magnitude distribution of the A901/902 supercluster sample of bright ($M_V < -18$), intermediate mass ($M > 1 \times 10^9 M_\odot$) galaxies (N=762 galaxies).

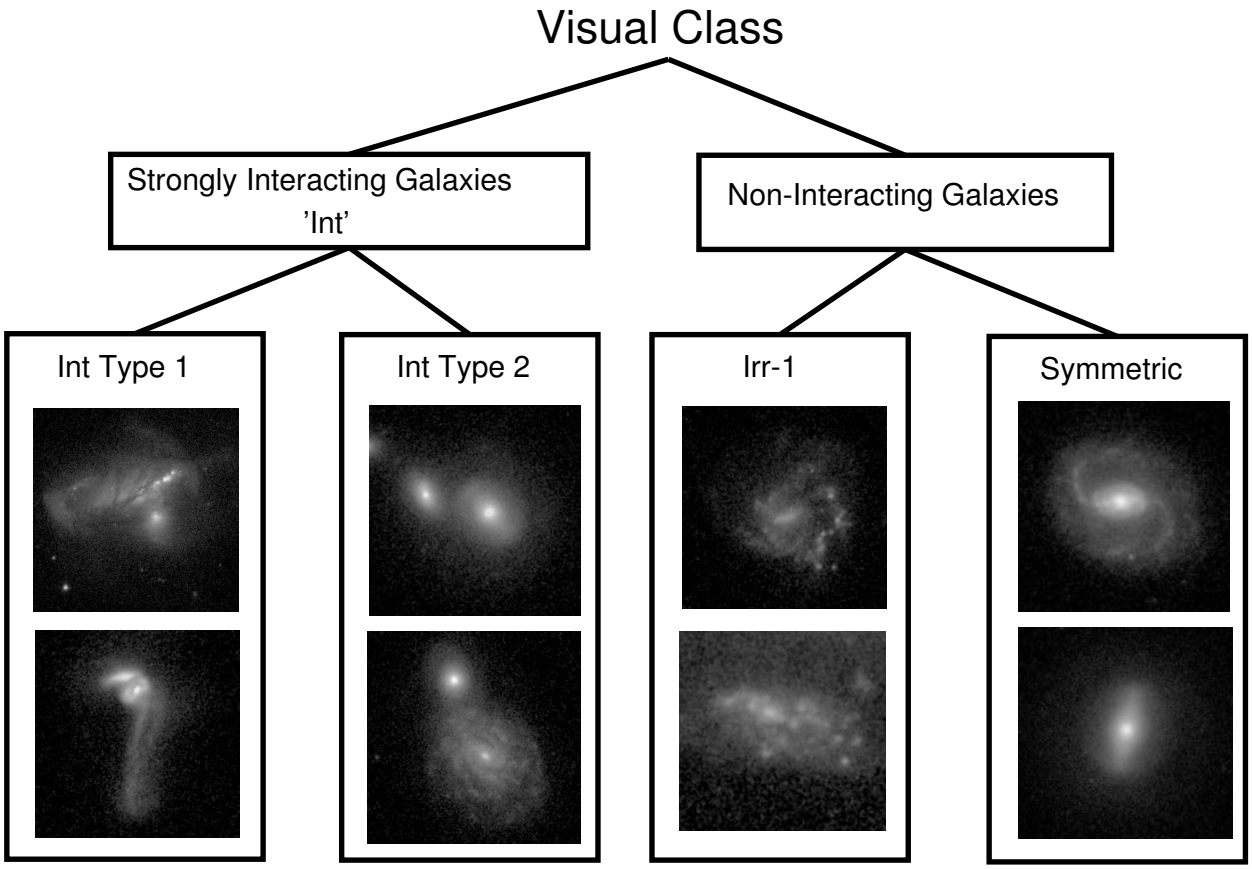

FIG. 2.— In our visual classification scheme (§ 3.2), galaxies are classified as interacting ('Int'), non-interacting, or unclassifiable. The interacting galaxies ('Int') consists of 'Type 1' and 'Type 2' systems (see Fig. 3). 'Int Type 1' systems host strong *externally-triggered* morphological distortions, such as tidal tails, shells, ripples, warps, asymmetric tidal debris and distortions in the disk, and double nuclei inside a common envelope. In contrast, 'Int Type 2' galaxies do not have strong morphological distortions, but they are considered to be interacting because they have a companion which satisfies 3 criteria: it has project separation d$\lesssim$10 kpc, the same COMBO-17 spectrophotometric redshift, and gives a stellar mass ratio $M_1/M_2 > 1/10$. The non-interacting galaxies consists of 'Irr-1' and 'Symmetric' systems. Irr-1 exhibit *internally-triggered* asymmetries, due to SF typically on scales of a few hundred parsecs. 'Symmetric' systems are relatively undistorted and are not associated with any overlapping companion.

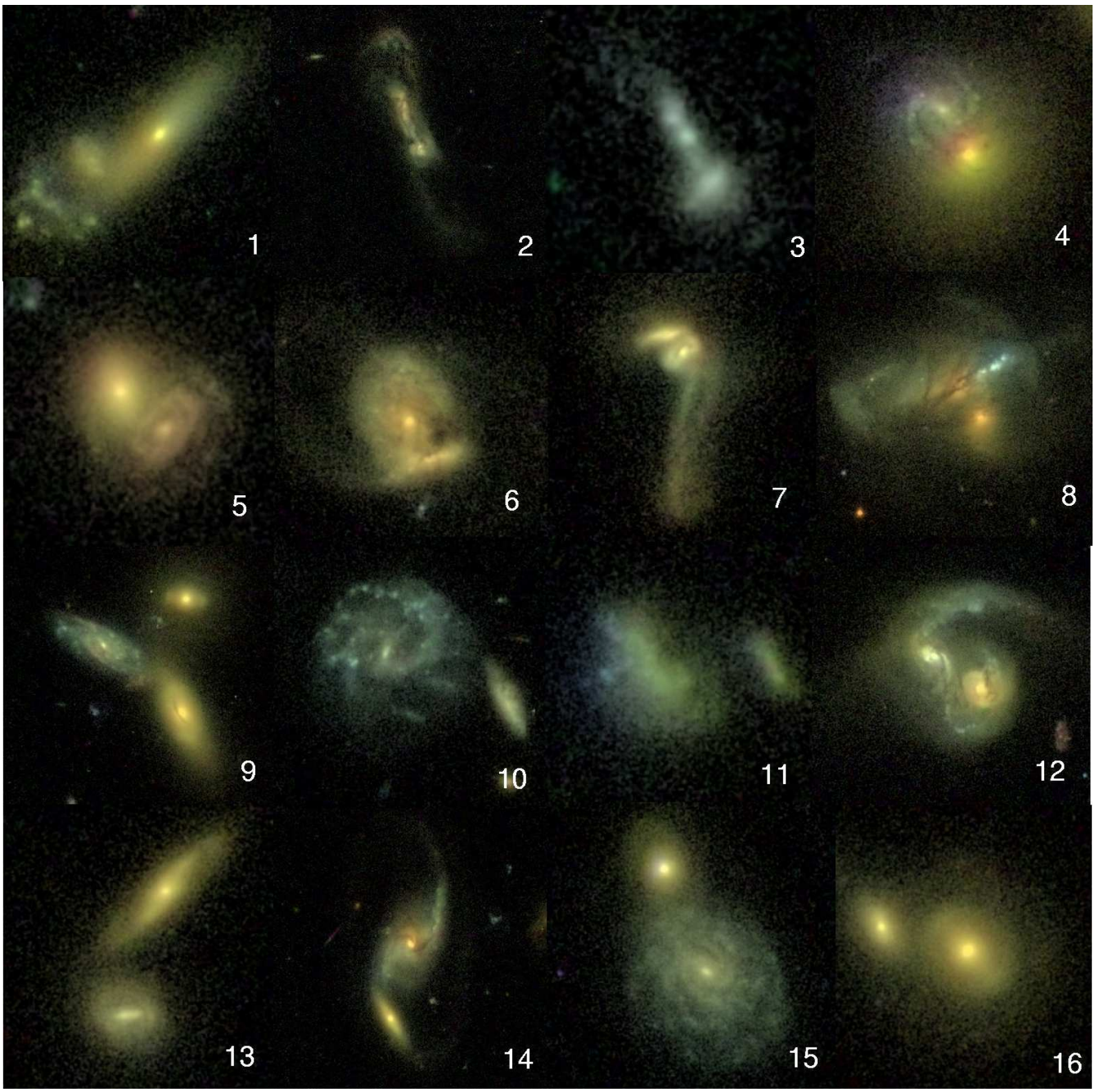

FIG. 3.— Examples of galaxies visually classified as interacting ('Int'), divided into 'Type 1' and 'Type 2' (§ 3.2). 'Int Type 1' systems (cases 1-8) host strong *externally-triggered* morphological distortions, such as tidal tails, arcs, shells, ripples, warps, tidal debris in body of galaxy, offset rings, extremely asymmetric star formation, spiral arms on only one side of the disk, and double nuclei. In contrast, 'Int Type 2' galaxies do not have strong morphological distortions (cases 9-11, 13-16), but they are considered to be interacting because they have a companion which satisfies 3 criteria: it has project separation d$\lesssim$10 kpc, the same COMBO-17 spectrophotometric redshift, and gives a stellar mass ratio $M_1/M_2 > 1/10$. Among these interacting systems, note potential major (9, 12, 13, 14, 15) and minor (10, 11, 16) interactions, as well as more ambiguous cases (1-8) that could be either major or minor (§ 4.1).

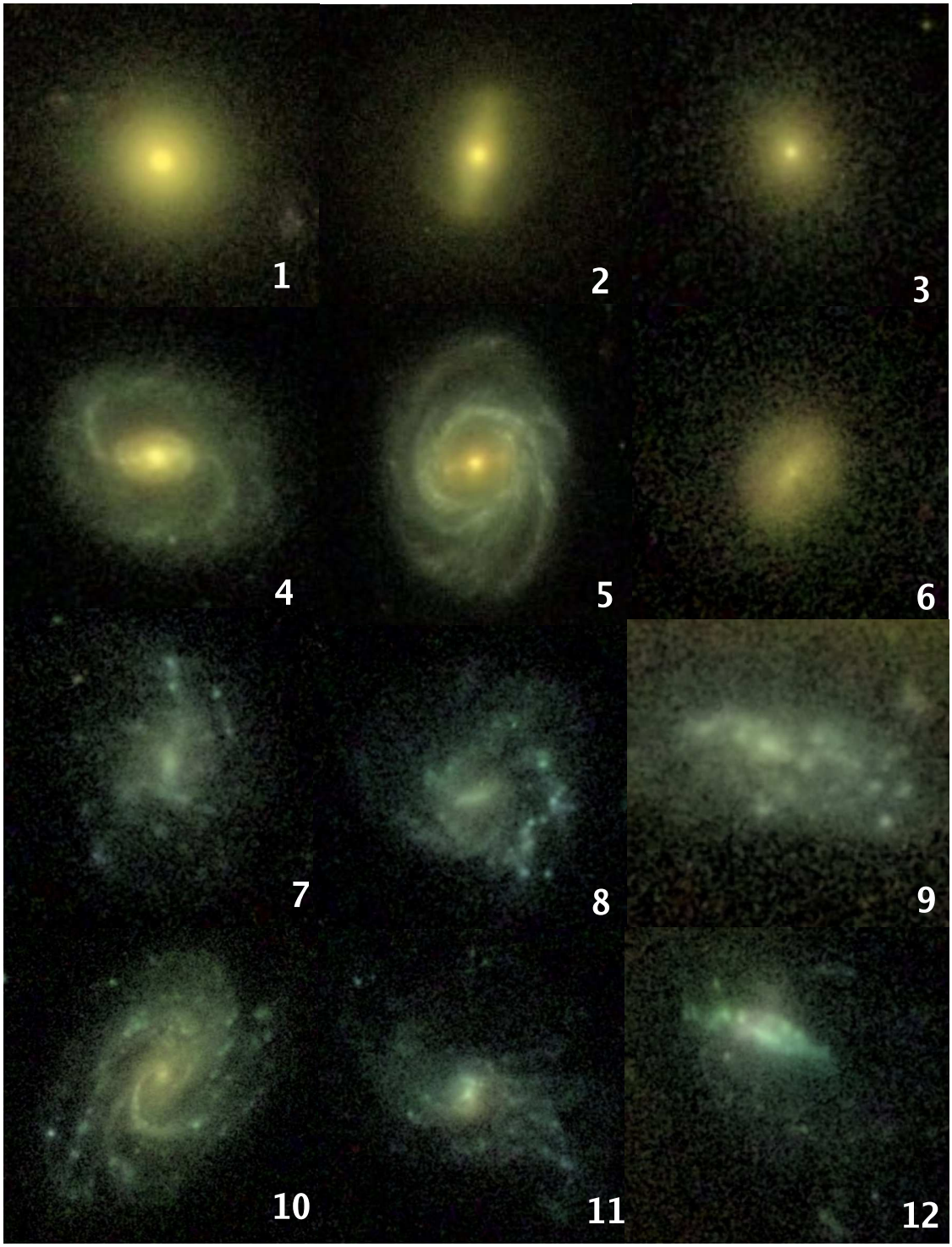

FIG. 4.— Examples of galaxies visually classified as Non-interacting Symmetric (cases 1-6) and Non-interacting Irr-1 (cases 7-12). See § 3.2 for details.

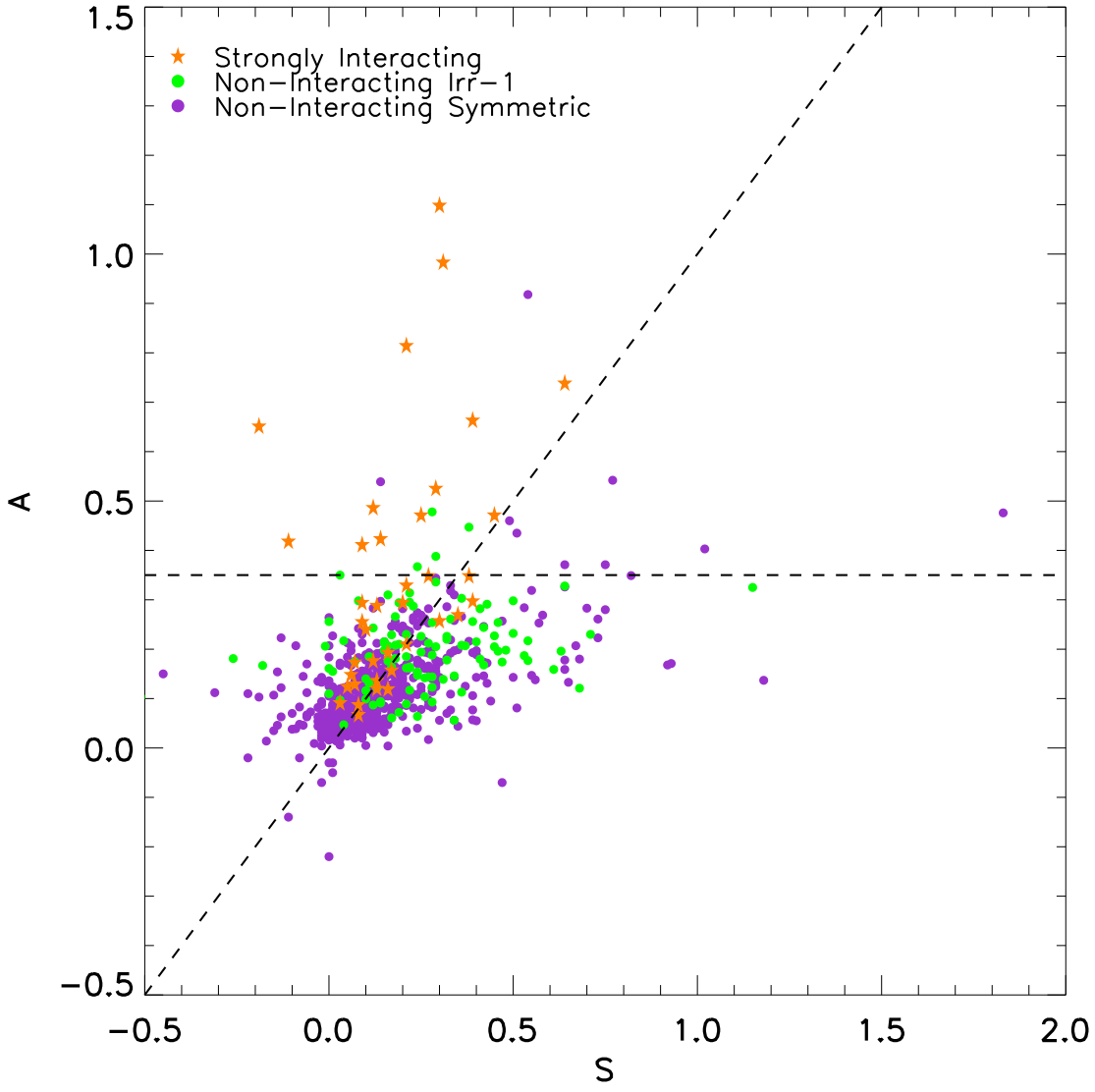

FIG. 5.— Bright, intermediate mass ($M_V < -18; M \geq 1 \times 10^9 M_\odot$) galaxies of different visual classes (Interacting, Non-interacting Irr-1, & Non-interacting Symmetric) are shown in the CAS A versus S plane. The 19 galaxies satisfying the CAS merger criterion ($A > S$ and $A > 0.35$) lie on the upper left corner of the diagram. The CAS merger criterion recovers 13/38 ($34^{+5\%}_{-0\%}$) of the galaxies visually classified as interacting. Furthermore, there is a significant level of contamination: 6/19 ($33^{+24\%}_{-4\%}$) of the systems picked up by the CAS criterion are visually classified as Non-interacting Irr-1 and Non-interacting Symmetric.

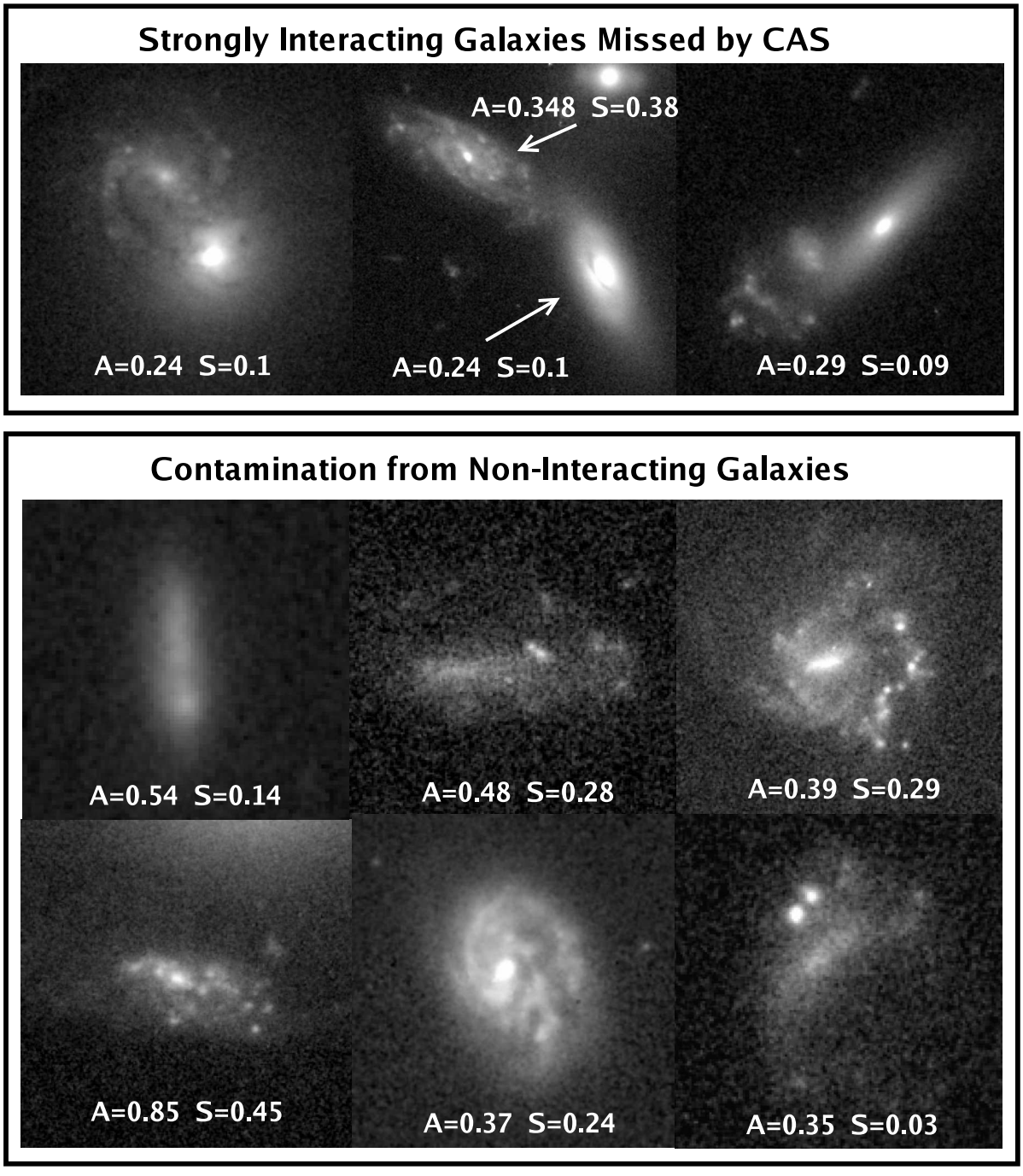

FIG. 6.— The top panel shows examples of interacting missed by CAS criterion ($A > S$ and $A > 0.35$). Features of these systems include double nuclei, tidal bridges, and tidal debris. The lower panel show some 'Non-Interacting' contaminants CAS picked up due to small-scale asymmetries from SF, large dust lanes, and the absence of a clear center, all leading to a larger A value.

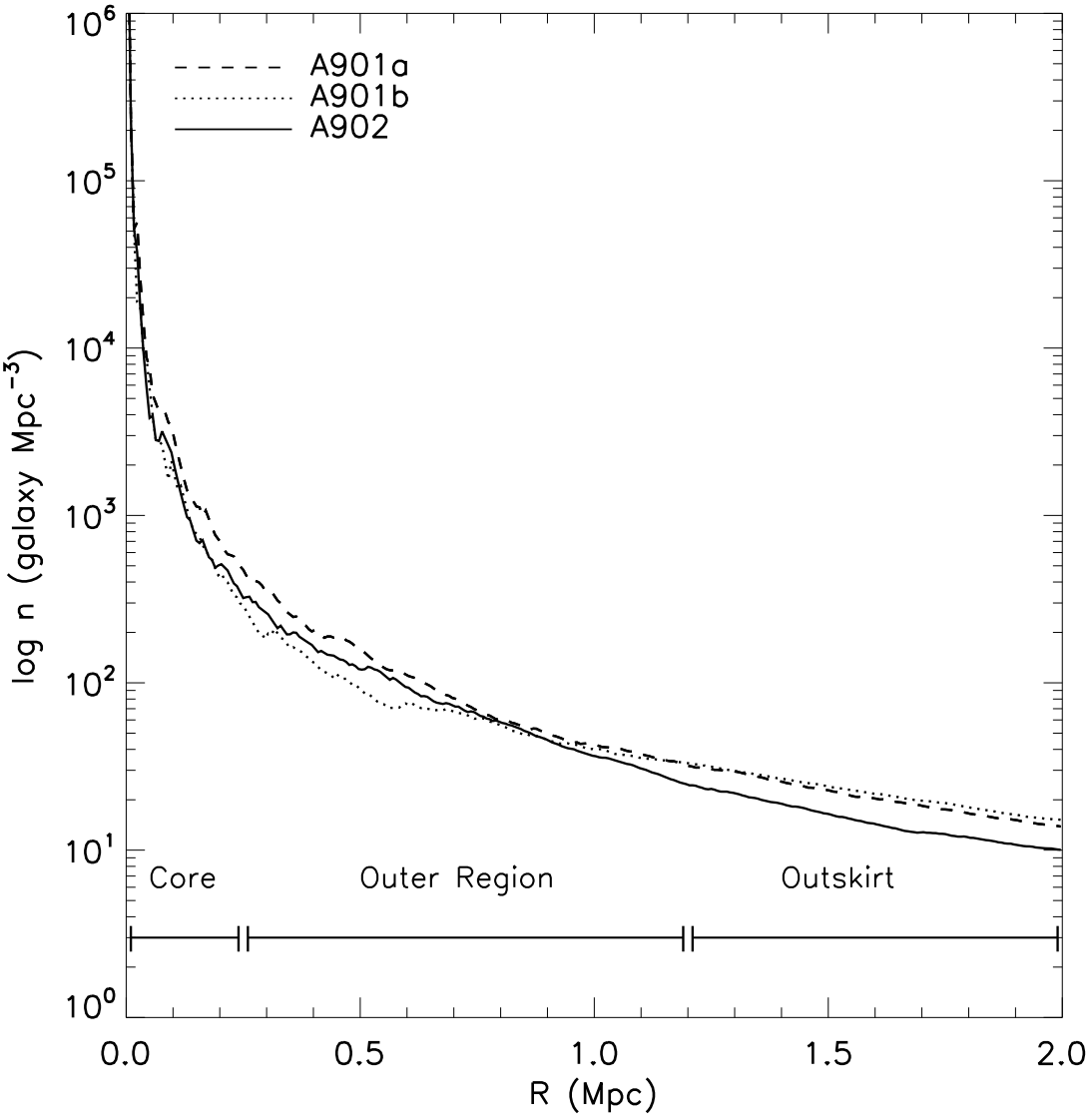

FIG. 7.— The azimuthally averaged projected number density n of bright ($M_V < -18$) galaxies as a function of clustocentric radius is shown for each cluster A901a/b and A902. We consider the cluster core to be at $R \leq 0.25$ Mpc, as this is the region where the projected number density n rises very steeply. We refer to the region which is located at 0.25 Mpc $< R \leq 1.2$ Mpc between the cluster core and the cluster virial radius as the 'outer region of the cluster'. The region outside the virial radius (1.2 Mpc $< R \leq 2.0$ Mpc) is referred to as the 'outskirt region of the cluster'. The core, outer region, and outskirt region are labeled.

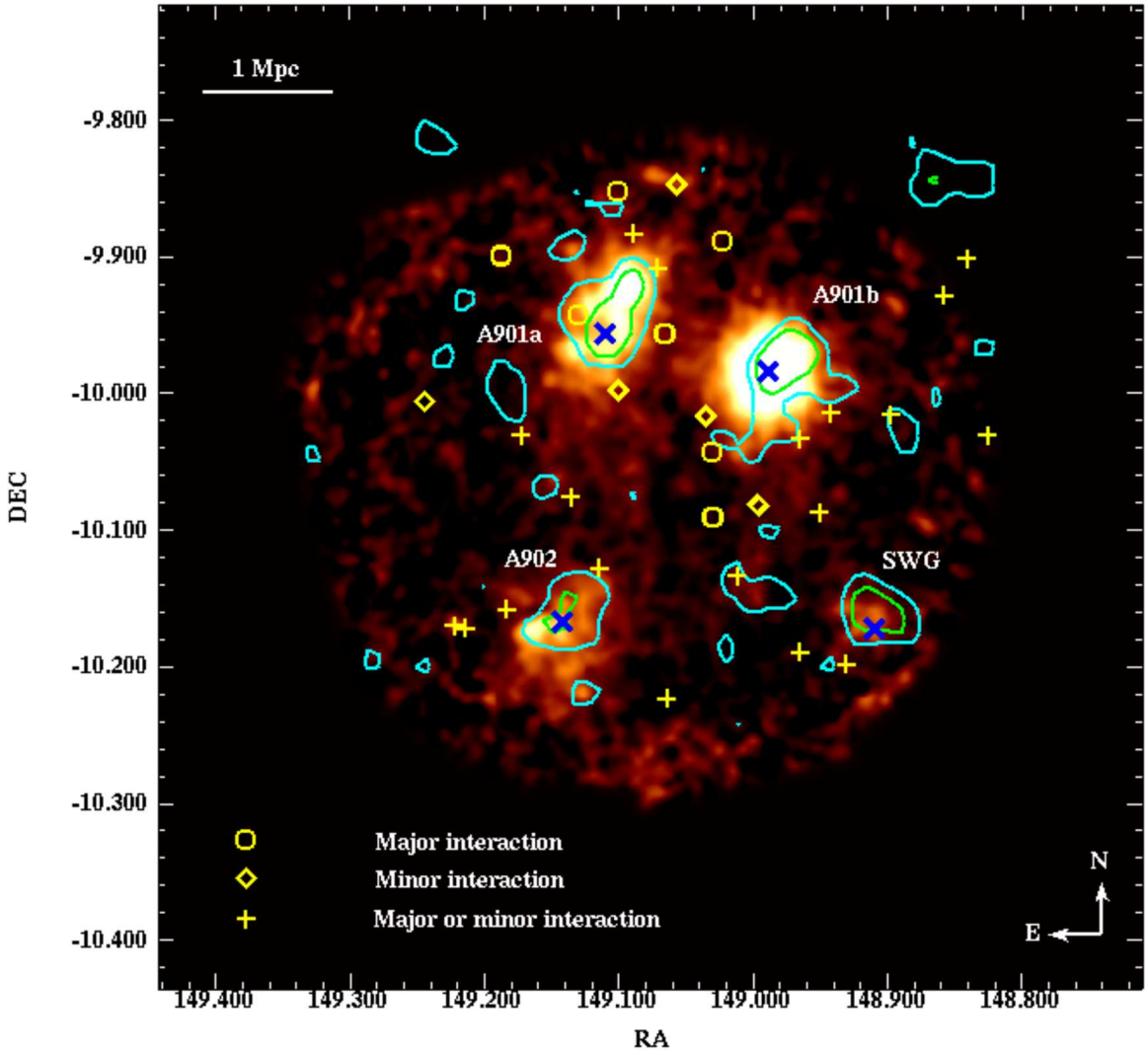

FIG. 8.— The distribution of interacting galaxies (coded as yellow diamonds, '+', and circles) is overlaid on the ICM density map (yellow-orange scale). Following Heymans et al. (2008), we show DM masses in terms of the signal-to-noise of the weak lensing detection. The cyan and green contours enclose roughly $6h^{-1}10^{13}M_{\odot}$ and $3.5h^{-1}10^{13}M_{\odot}$ for A901a and A901b, and roughly $3h^{-1}10^{13}M_{\odot}$ and $1.5h^{-1}10^{13}M_{\odot}$ for the lower mass A902 and South West Group (SWG). The different symbols represent our best attempt to separate the interacting galaxies into 'major' (circles), 'minor' (diamonds), and 'major or minor' (+) interactions (§ 4.3). Interacting galaxies are located in the outer region of each cluster (0.25 Mpc $< R \leq$ 1.2 Mpc).

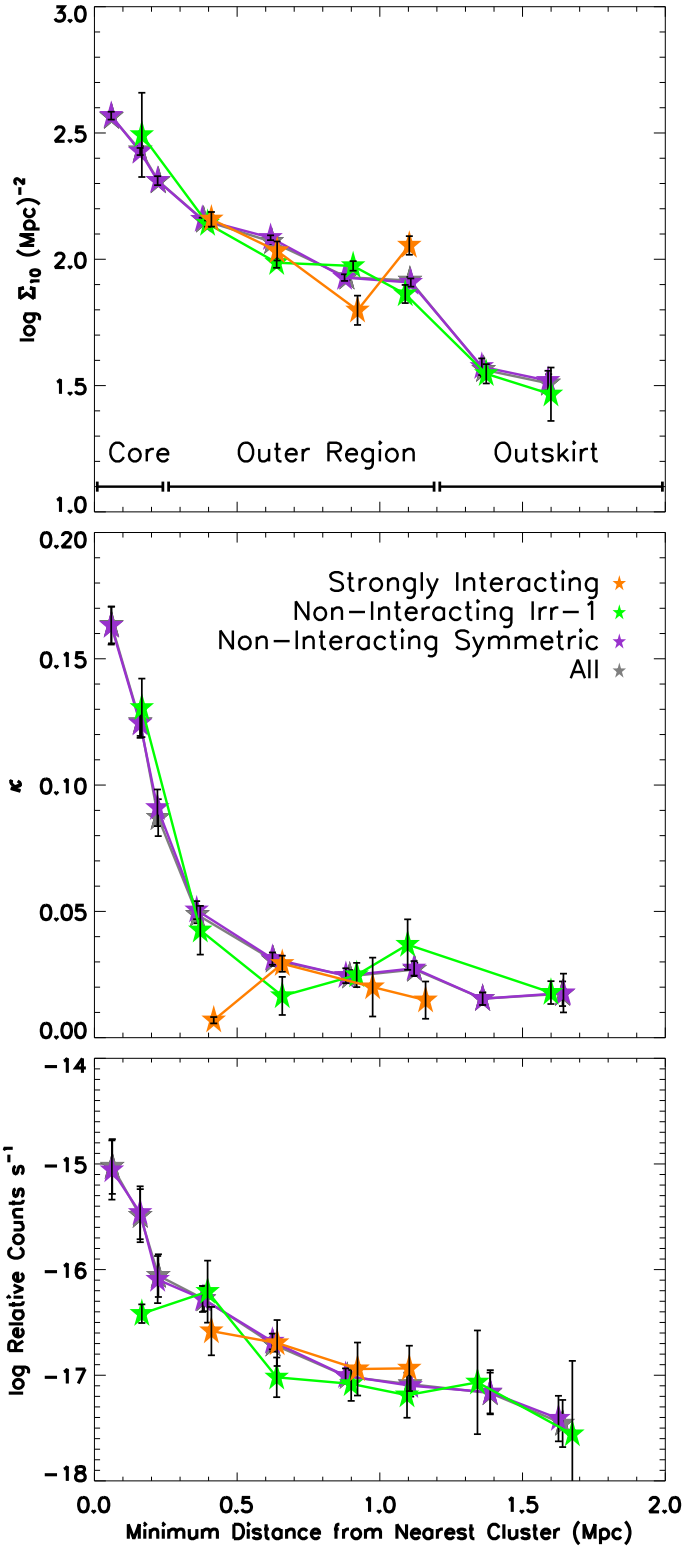

FIG. 9.— The distribution of local galaxy surface density Σ_{10} **(top)** local DM mass surface density κ **(middle)**, and relative local ICM density **(bottom)** is shown as a function of the minimum distance from the nearest cluster center (A901a, A901b, A902, SWG), for bright galaxies of different visual classes : Interacting, Non-interacting Irr-1, and Non-interacting Symmetric. Since the interacting galaxies lie preferentially in the outer region of the cluster (0.25 Mpc $< R \leq$ 1.2 Mpc), they are associated with low values of κ and intermediate values of Σ_{10}, and ICM density.

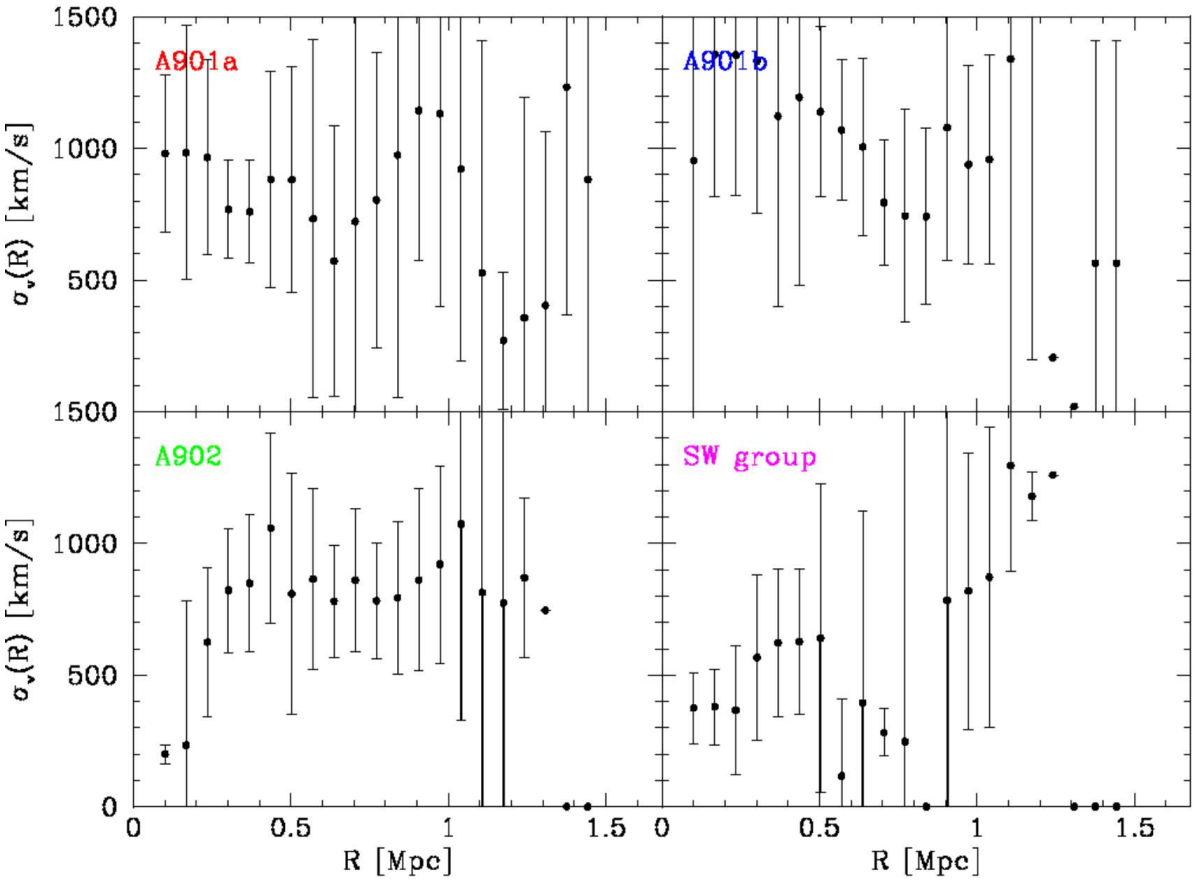

FIG. 10.— Local velocity dispersion profiles for A901a, b and A902 clusters, and associated SWG from kinematic modeling using the ~ 300 2dF redshifts (Gray et al. in prep.). The central galaxy velocity dispersion within the cores ($R < 0.25$ Mpc) of A901a,b and A902 typically range from 700 to 1000 km s^{-1}. Outside the cluster core, in the outer region (0.25 Mpc $< R \leq 1.2$ Mpc), the small number statistics leads to large error bars on the galaxy velocity dispersion, making it un-viable to determine whether it remains high or drops.

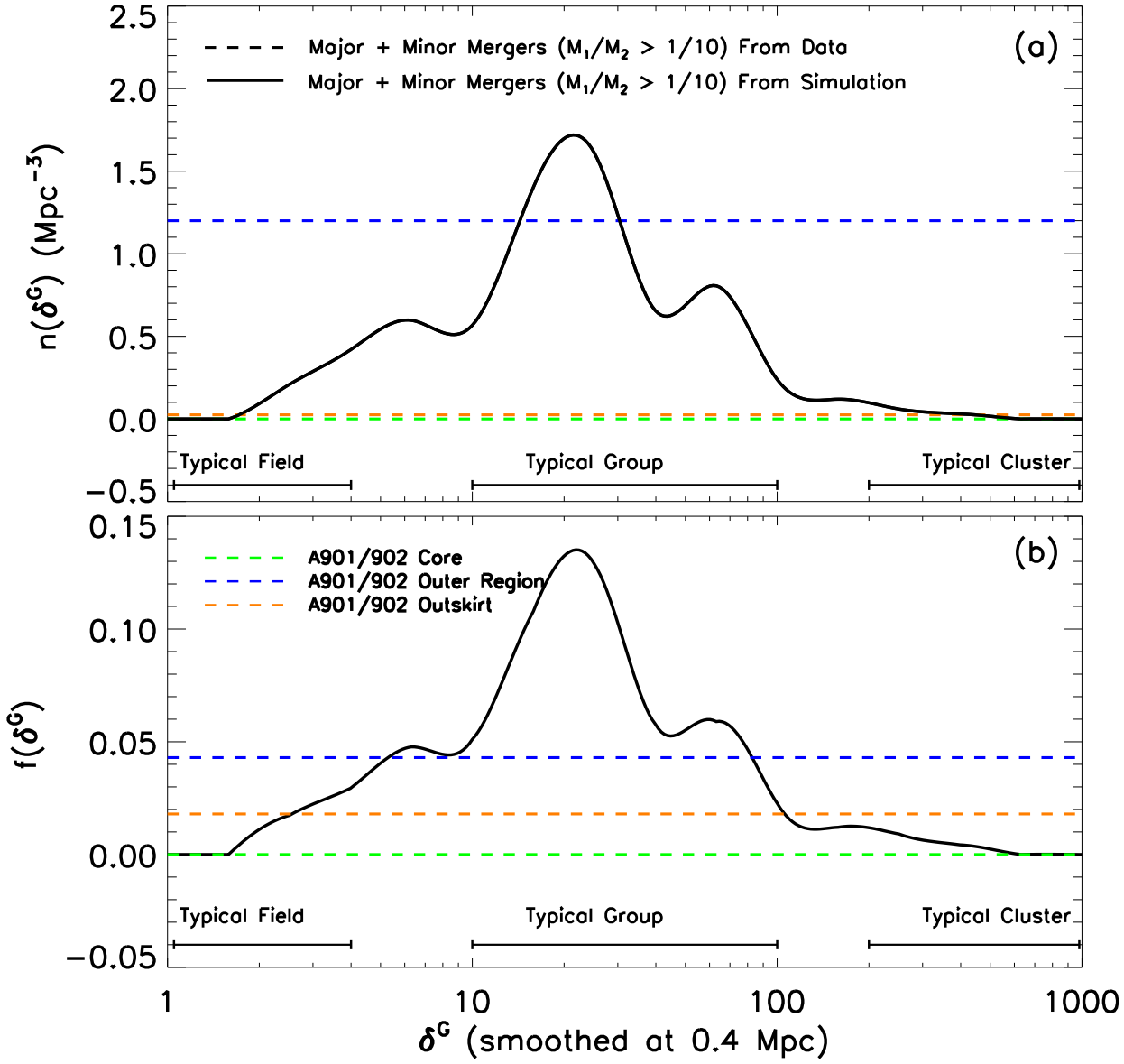

FIG. 11.— The solid curve shows the model predictions, from N-body simulations of the STAGES A901/902 supercluster (van Kampen et al. 2008, in prep.; see § 4.3 for details), for the number density, ($n(\delta^{\rm G})$; **a**) and fraction, ($f(\delta^{\rm G})$;**b**) of galaxy mergers of mass ratio $M_1/M_2 > 1/10$ as a function of local overdensity ($\delta^{\rm G}$). The latter is is calculated by smoothing the density of dark matter halos with a Gaussian of width 0.4 Mpc to takeout the effect of individual galaxies. Typical values of $\delta^{\rm G}$ are $\sim$ 10-100 for group overdensities, $\sim$ 200 at the cluster virial radius, and $\gtrsim$ 1000 in core of rich clusters. A stellar mass cut of ($M > 1\times 10^9\ M_\odot$) is applied to galaxies. As field and group galaxies fall into a cluster along filaments, the bulk flow enhances the galaxy density and causes galaxies to have small relative velocities, thus leading to a high probability for mergers at typical group overdensities. Closer to the cluster core, galaxies show large random motions, producing a sharp drop in the probability of mergers. The 3 dashed lines show the estimated observed number density ($n_{\rm merg}$) and fraction ($f_{\rm merg}$) of mergers, for the 3 different regions of the A901/902 clusters (core, outer region, and outskirt). The points at which the dashed lines cross the solid curve tell us the typical overdensities at which we expect to find such merger densities in the simulations. Between the cluster core and the cluster virial radius (0.25 Mpc $< R \leq$ 1.2 Mpc), the observed merger density is close to those seen at typical *group overdensities*, in agreement with the scenario of cluster growth via accretion of field and/or group galaxies.

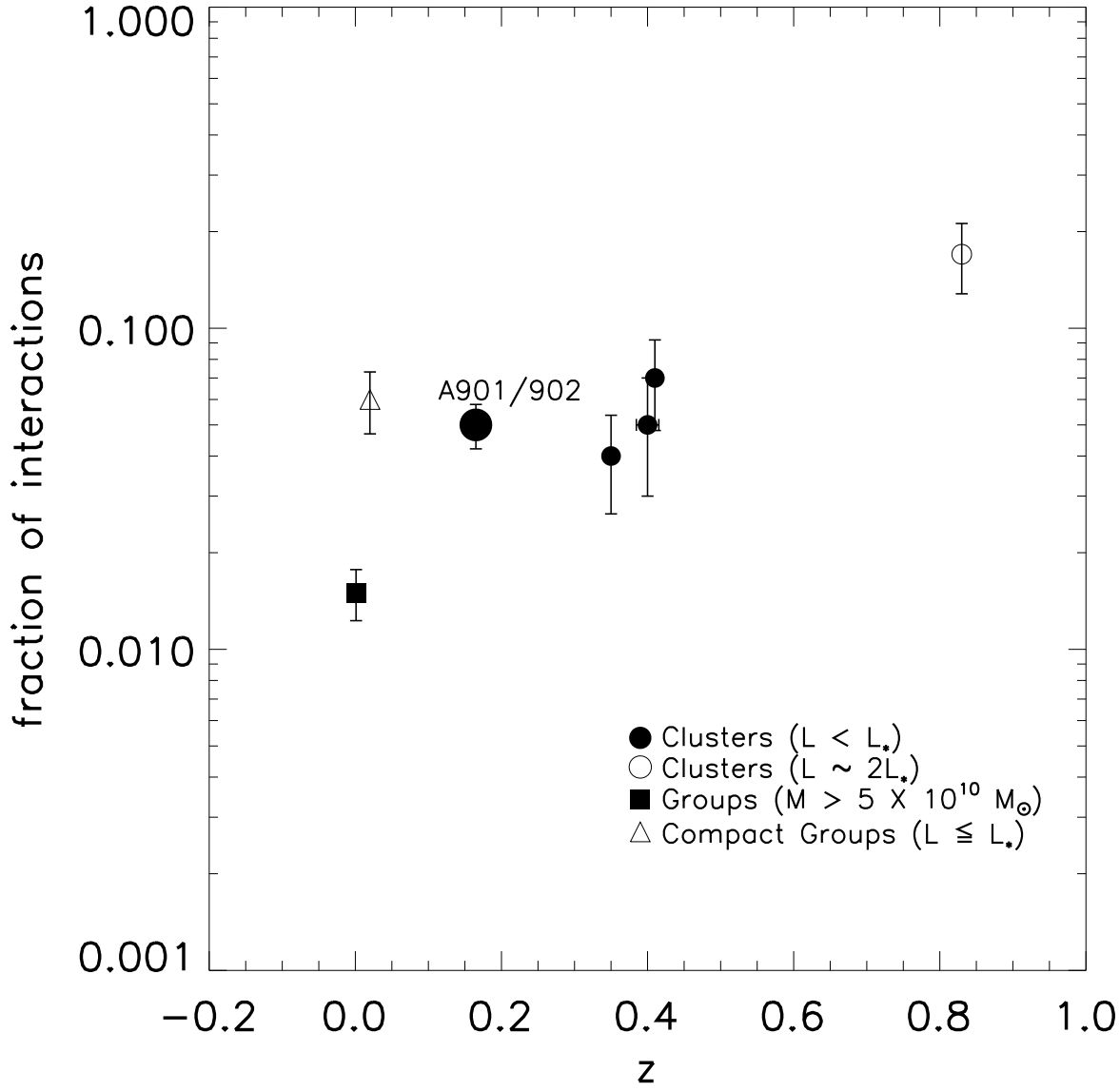

FIG. 12.— Comparisons of our observed fraction of interacting galaxies with other studies of clusters, groups, and field galaxies. Filled circles are for cluster data points of intermediate luminosity ($L < L^*$ and/or $M = 1 \times 10^9$ to a few $\times 10^{10} M_\odot$), and the cluster data points are in order of increasing redshift: this study of A901/902 (most systems have $M_V \sim -19$ to -22 and $M_* = 1 \times 10^9$ to a few $\times 10^{10} M_\odot$); Couch et al. (1998; $L < 2L^*$), Oemler et al. (1997; lower limit of f for $M_V < -19$), Dressler et al. (1994; $M_V < -18.5$). The van Dokkum et al. (1999) point at $z = 0.83$ (open circle) is for a cluster sample of luminous ($M_B \sim -22$ and $L \sim 2L^*$) galaxies. The group point (filled square) is from McIntosh et al. (2007) for galaxy masses above $5 \times 10^{10} M_\odot$. The Hickson compact group point (open triangle) is from Zepf et al. (1993) and is for galaxies of luminosities $L \leq L^*$.

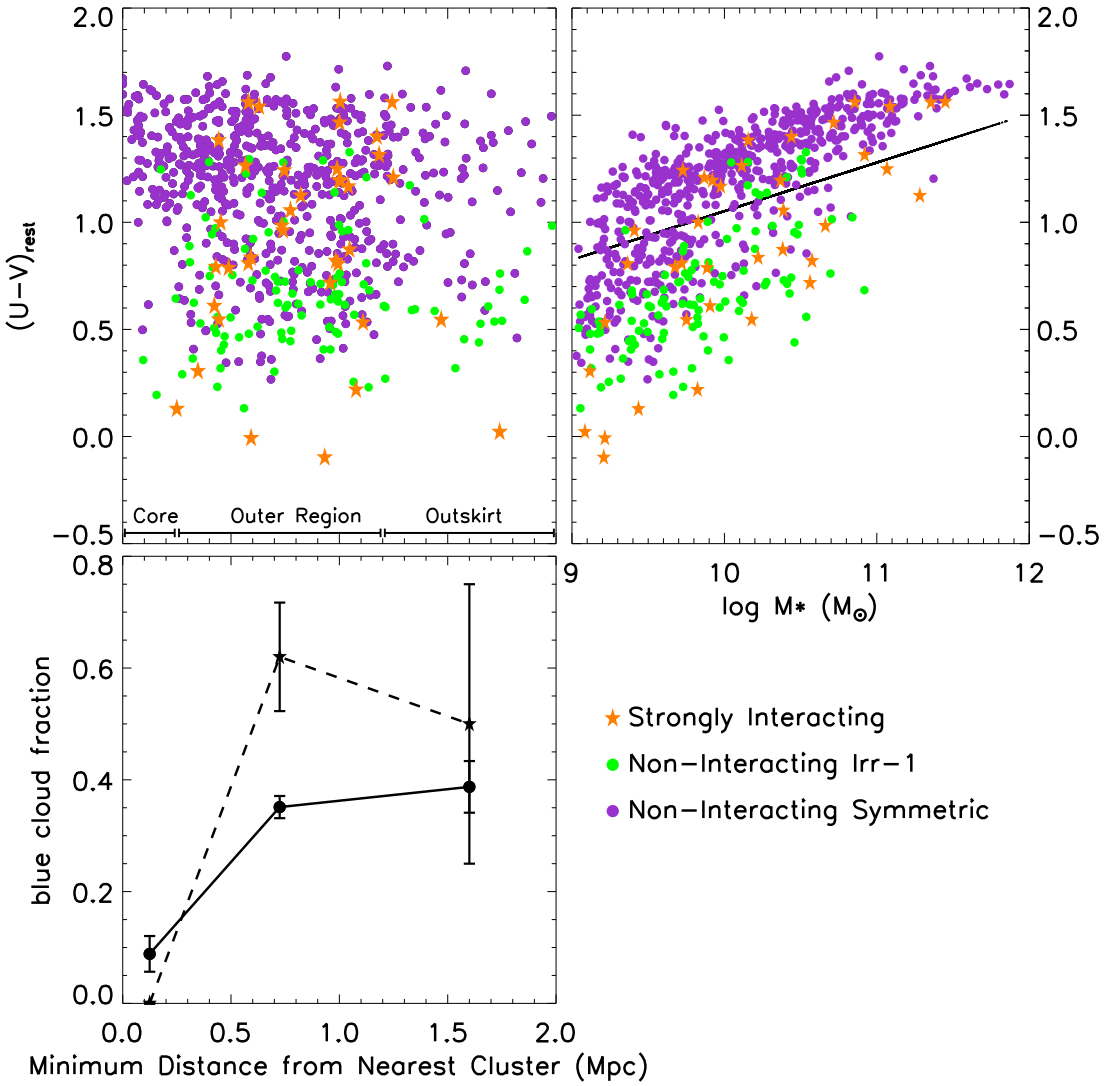

FIG. 13.— **Top Left:** The rest-frame $U-V$ color of galaxies is plotted against their minimum distance from the nearest cluster center. **Top Right:** The rest-frame $U-V$ color is plotted against stellar masses for galaxies of different visual classes (Interacting, Non-interacting Irr-1, and Non-interacting Symmetric). The black solid lines separate the blue cloud and red sequence. For $M \geq 1 \times 10^9 M_{\odot}$ systems, we find that $61 \pm 14\%$ (23/38) of the interacting galaxies lie on the blue cloud, compared to $35 \pm 7\%$ (251/720) for non-interacting galaxies. There is an excess of blue galaxies among interacting systems. **Bottom Left:** The fraction of all galaxies on the blue cloud (solid line), and the fraction of interacting galaxies on the blue cloud (dotted line) both rise as a function of clustocentric radius (Table 7). The increase is more pronounced for the fraction of blue interacting galaxies, which rises from 0 to 0.62 ± 0.15 to $0.50 \pm 0.25\%$ (Table 7) in the cluster core ($R \leq 0.25$ Mpc) to the outer region (0.25 Mpc $< R \leq 1.2$ Mpc) to the outskirt region (1.2 Mpc $< R \leq 2$ Mpc).

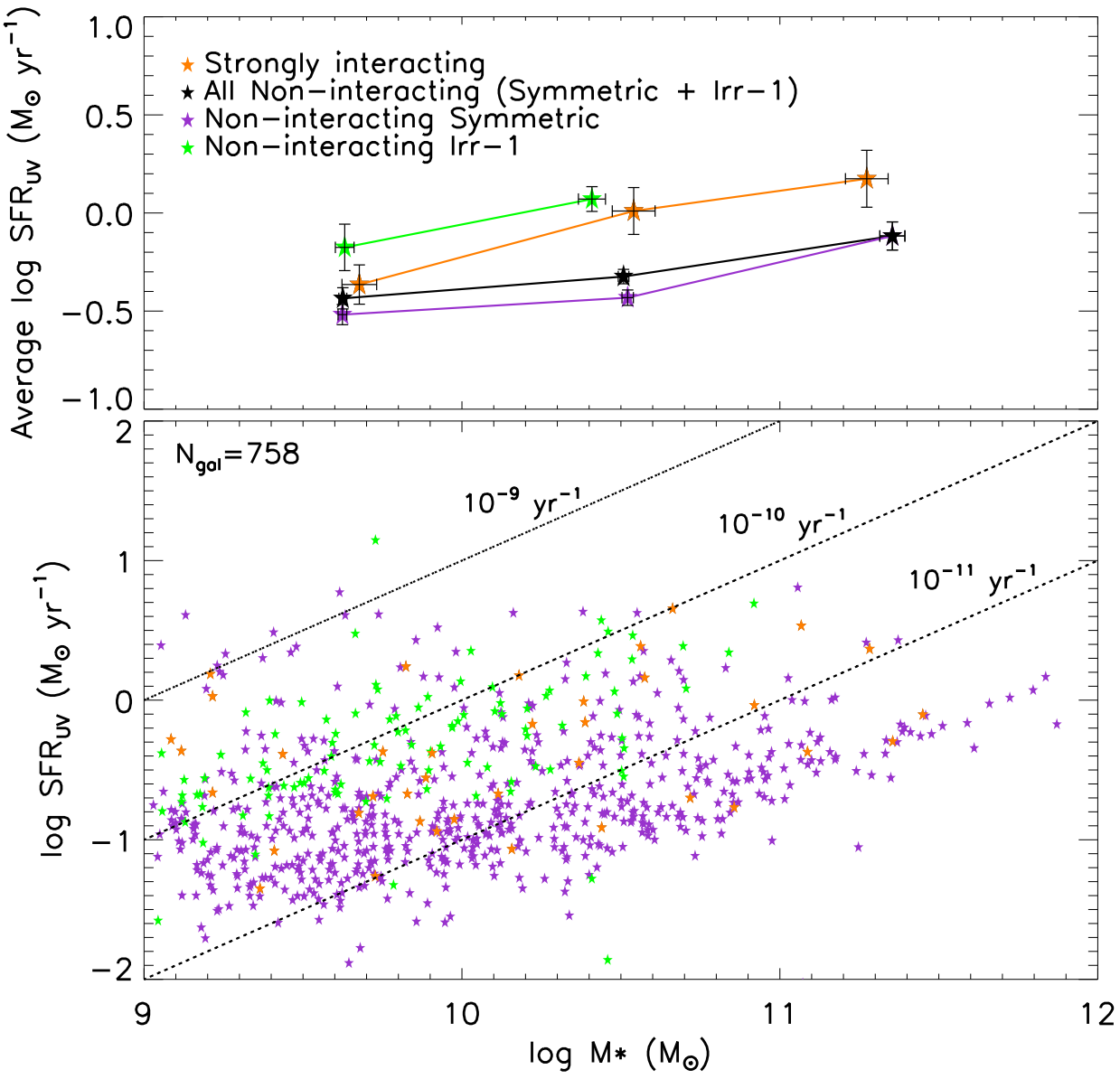

FIG. 14.— **Lower panel:** The UV-based SFR is plotted versus stellar mass. Galaxies are coded according to their visual classes: Interacting, Non-interacting Irr-1, and Non-interacting Symmetric. Loci of constant specific SFR are marked in units of yr^{-1}. **Top panel:** The average UV-based SFR is plotted versus stellar mass for galaxies of different visual classes. For the few interacting galaxies present (orange line), the average SFR$_{UV}$ is enhanced by at most a modest factor of 1.2-2.2 compared to the Non-interacting Symmetric galaxies (purple line) and to all Non-interacting galaxies (i.e Symmetric + Irr-1; black line). No enhancement is seen with respect to the Non-interacting Irr-1 galaxies (green line).

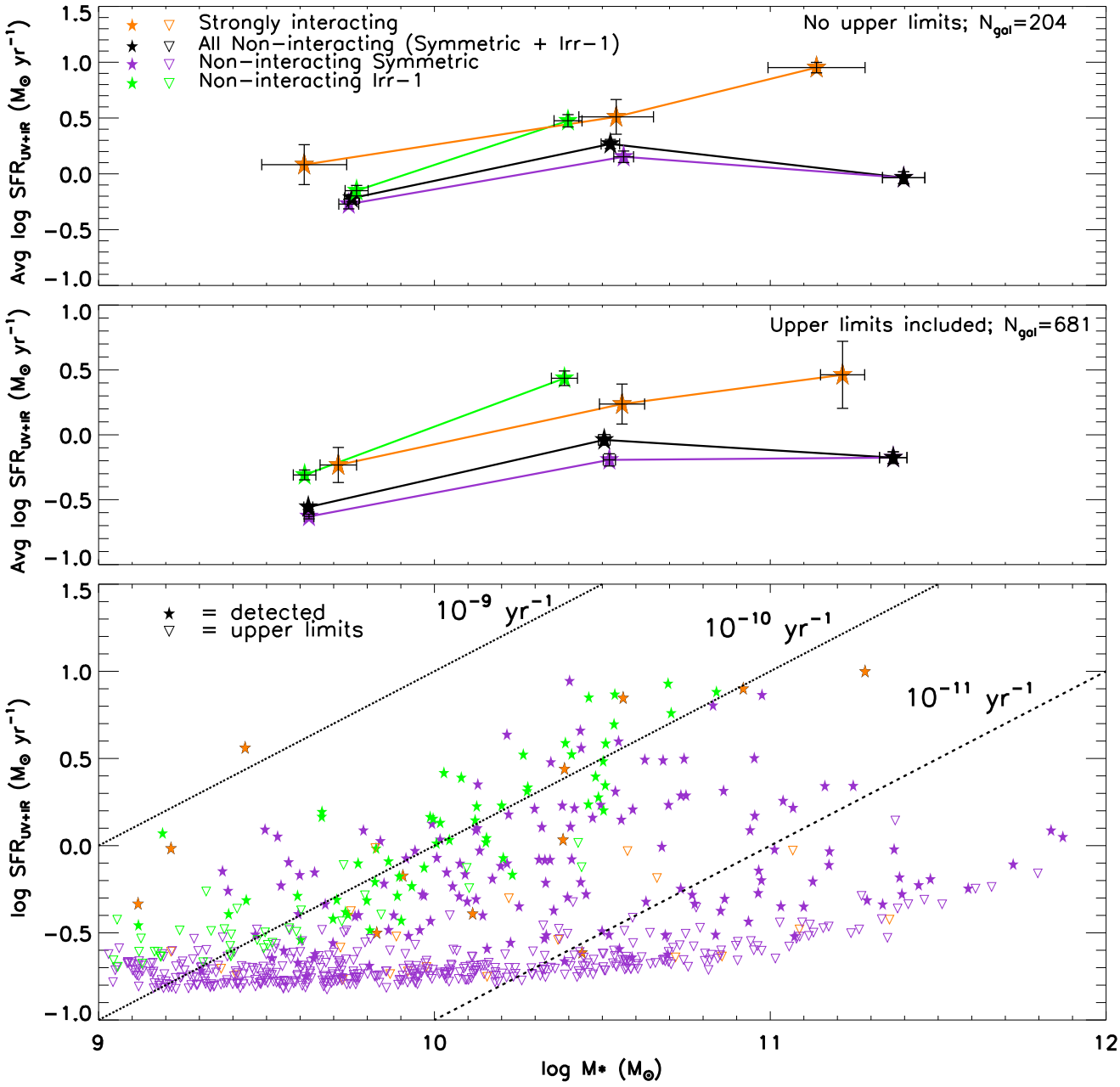

FIG. 15.— **Bottom panel:** The UV+IR-based SFR is plotted versus stellar mass. Galaxies are coded according to their visual classes: Interacting, Non-interacting Irr-1, and Non-interacting Symmetric. Loci of constant specific SFR are marked in units of yr^{-1}. The inverted triangles denote upper limits on the UV+IR-based SFR for galaxies for which there was no 24μm detection and we used the detection limit. **Middle panel:** The average UV+IR-based SFR is plotted versus stellar mass for galaxies of different visual classes. We include galaxies with a 24μm detection, as well as those with only upper limits on the 24μm flux. **Top panel:** Same as middle panel, except that we only include galaxies with a 24μm detection and exclude those with upper limits. In both top and middle panel, we find that for the few interacting galaxies present (orange line), the average SFR_{UV+IR} is typically enhanced by only a factor of $\sim$ 2 to 3 compared to the Non-interacting Symmetric galaxies (purple line) and to all Non-interacting galaxies (i.e Symmetric + Irr-1; black line).